AFWAL-TR-88-4245

DEVELOPMENT OF A SEMIQUANTITATIVE CORROSION MONITOR

FRANK ANSUINI

DYNACO CORPORATION
P.O. BOX 3209
DERRY, NH 03038

FEBRUARY 1989

Final Report for Period October 1985 to October 1988

MATERIALS LABORATORY
AIR FORCE WRIGHT AERONAUTICAL LABORATORIES
AIR FORCE SYSTEMS COMMAND
WRIGHT-PATTERSON AIR FORCE BASE, OHIO 45433-6533

REPORT DOCUMENTATION PAGE

Form Approved OMB No. 0704-0188

1a. REPORT SECURITY CLASSIFICATION: UNCLASSIFIED	1b. RESTRICTIVE MARKINGS: N/A
2a. SECURITY CLASSIFICATION AUTHORITY: N/A	3. DISTRIBUTION/AVAILABILITY OF REPORT: Approved for public release; distribution unlimited.
2b. DECLASSIFICATION/DOWNGRADING SCHEDULE: N/A	
4. PERFORMING ORGANIZATION REPORT NUMBER(S): N/A	5. MONITORING ORGANIZATION REPORT NUMBER(S): AFWAL-TR-88-4245
6a. NAME OF PERFORMING ORGANIZATION: Dynaco Corp. / 6b. OFFICE SYMBOL (If applicable): N/A	7a. NAME OF MONITORING ORGANIZATION: Materials Laboratory
6c. ADDRESS (City, State, and ZIP Code): PO Box 3209 Derry, NH 03038	7b. ADDRESS (City, State, and ZIP Code): AFWAL/MLSA Wright-Patterson AFB, OH 45433-6533
8a. NAME OF FUNDING/SPONSORING ORGANIZATION: AFWAL (SBIR) / 8b. OFFICE SYMBOL (If applicable): MLSA	9. PROCUREMENT INSTRUMENT IDENTIFICATION NUMBER: F33615-85-C-5069
8c. ADDRESS (City, State, and ZIP Code): WPAFB OH 45433-6533	10. SOURCE OF FUNDING NUMBERS

PROGRAM ELEMENT NO.	PROJECT NO.	TASK NO.	WORK UNIT ACCESSION NO.
65502F	3005	50	34

11. TITLE (Include Security Classification)

Development of a Semiquantitative Corrosion Monitor

12. PERSONAL AUTHOR(S)
Frank Ansuini

13a. TYPE OF REPORT	13b. TIME COVERED	14. DATE OF REPORT (Year, Month, Day)	15. PAGE COUNT
Final	FROM Oct 85 TO Oct 88	1989/2/6	59

16. SUPPLEMENTARY NOTATION

N/A

17. COSATI CODES			18. SUBJECT TERMS (Continue on reverse if necessary and identify by block number)
FIELD	GROUP	SUB-GROUP	
01	1106		Test methods, Corrosion Testing, Atmospheric Corrosion.
02	0903		

19. ABSTRACT (Continue on reverse if necessary and identify by block number)

This report describes a prototype dual mode corrosion monitor which is capable of measuring both instantaneous corrosion rate and cumulative corrosion loss in atmospheric environments not boldly exposed to weather. The monitor system consists of two components: a small flat sensor to be located in the area to be monitored and a battery powered electronics unit to query the sensor. The sensor element is made of steel which is far more sensitive to atmospheric corrosion than most commonly used metals; thus the sensor will react before significant damage has been done to other materials. The sensor itself is actually two discrete sensors on the same substrate and photo-etched from the same foil. Corrosion rate is measured using two-electrode

(Continued)

20. DISTRIBUTION/AVAILABILITY OF ABSTRACT	21. ABSTRACT SECURITY CLASSIFICATION
☒ UNCLASSIFIED/UNLIMITED ☐ SAME AS RPT. ☐ DTIC USERS	UNCLASSIFIED

22a. NAME OF RESPONSIBLE INDIVIDUAL	22b. TELEPHONE (Include Area Code)	22c. OFFICE SYMBOL
FRED H. MEYER, JR.	(513) 255-5117	AFWAL/MLSA

DD Form 1473, JUN 86 — Previous editions are obsolete. — SECURITY CLASSIFICATION OF THIS PAGE

Block 19 - ABSTRACT (continued)

Linear Polarization Resistance (LPR) while cumulative loss is measured by the Electrical Resistance (ER) method. The electronics unit has been designed for operation by personnel with minimal corrosion knowledge. Its primary purpose is to alert an operator of the existence of corrosive conditions so that remedial action can be taken before extensive corrosion damage has occurred.

EXECUTIVE SUMMARY

The prototype dual mode corrosion monitor developed under this project is capable of measuring both instantaneous corrosion rate occurring at time of measurement and cumulative corrosion loss which has occurred since the sensor was first installed. Both types of measurements are needed to properly monitor corrosion. Rate measurements define the severity of a corrosion problem and are often the first indication of an abnormal situation. Loss measurements serve as a back-up for rate measurements by maintaining a record of the total amount of corrosion damage which has occurred since the sensor was first installed.

The monitor system consists of two components: a small flat transducer or sensor to be located in the area to be monitored and a battery powered electronics unit to query the sensor. The model developed during this project is designed to monitor atmospheric environments not boldly exposed to weather. Typical applications would be electronics spaces and storage enclosures. The sensor element is made of steel which is far more sensitive to atmospheric corrosion than most other metals; thus the sensor will react before significant damage has been done to the primary materials.

The sensor itself is actually two discrete sensors on the same substrate and photoetched from the same foil. Corrosion rate is measured by the two-electrode Linear Polarization Resistance (LPR) technique. The LPR sensor consists of two interdigitated electrodes separated by a 3 mil gap. A 20 mV bias potential is applied between the electrodes; the quantity of current which flows is proportional to the instantaneous corrosion rate.

Cumulative corrosion loss is measured by the Electrical Resistance (ER) method. The electrical resistance of a single electrode is measured. As this electrode thins from corrosion, its resistance proportionately increases. Temperature variations in resistivity is compensated by providing a second electrode with similar initial resistance but which is shielded from the environment. The circuit measures the increase in the resistance of the active electrode relative to that of the dummy electrode.

The electronics unit has been designed for operation by personnel with minimal corrosion knowledge. Its primary purpose is to alert an operator of the existence of corrosive conditions so that remedial action can be taken before extensive corrosion damage has occurred.

PREFACE

This report is prepared under Phase 2 SBIR contract to Dynaco Corp., PO Box 3209, Derry, NH 03038. Contracting agency is AFWAL/MLSA; Contract No. F33615-85-C-5069. It represents a continuation of effort begun under Phase 1 SBIR Contract F33615-83-C-5104. The program objective is to develop a highly sensitive semiquantitative corrosion monitor based on technology demonstrated in the Phase 1 program. Six discrete tasks comprise the program as enumerated below:

Task 1 - Test facilities preparation
Task 2 - Sensor design refinement
Task 3 - Packaging study
Task 4 - Electronics development
Task 5 - Qualification tests
Task 6 - Long term testing

Work performed under Tasks 1 and 2 was reported in Interim Report No. 2 in December, 1966. This report describes the work performed under the remaining tasks and is organized as follows:

Section 1 - Introduction
Section 2 - Packaging Test Results
Section 3 - Final Sensor Design
Section 4 - Electronic Design
Section 5 - System Response
Section 6 - Future Work

1.0 INTRODUCTION

Background

Two quantities are of interest in the field of corrosion monitoring: the instantaneous corrosion rate occurring at the time of measurement and the cumulative corrosion loss which has occurred since the sensor was first installed. Both types of measurements are needed to properly monitor corrosion. Rate measurements define the severity of a corrosion problem and are often the first indication of an abnormal situation. Loss measurements serve as a backup for rate measurements by maintaining a record of the total amount of corrosion damage which has occurred over some time interval.

Corrosion rate is frequently monitored by using the two-electrode Linear Polarization Resistance (LPR) technique. An LPR sensor is typically two electrodes between which a small bias potential is applied. The quantity of current which flows between the electrodes in response to the applied potential is proportional to the instantaneous corrosion rate.

Cumulative corrosion loss is often determined by the Electrical Resistance (ER) method. The electrical resistance of a single electrode exposed to the environment of interest is measured. As this electrode thins from corrosion, its resistance proportionately increases. Temperature variations in resistivity are compensated by providing a second electrode of the same material and initial resistance but which is shielded from the environment. The measurement circuit, therefore, measures the increase in the resistance of the active electrode relative to that of the dummy electrode.

Existing corrosion monitoring equipment will typically use only one of these techniques. If both rate and loss information is desired, it is necessary to install two separate monitoring systems. The cost of corrosion monitoring could be reduced if a single corrosion sensor could be designed which was capable of measuring both rate and loss. We had proposed that such a sensor could be made using the photofabrication process. The sensor itself is actually two discrete sensors on the same substrate and photo-etched from the same foil.

During a Phase 1 SBIR contract, in which the feasibility of this concept was demonstrated, the pattern shown in Figure 1 was prepared [1]. Sensors were produced by etching this pattern into foils of several different metals. The thickness of the metal foils used was limited to that which was readily available and was far from the optimum for this application. In addition, the same trace pattern was used on all four metals tested rather than tailoring the pattern to the properties of the metal being tested. The use of a single "compromise" pattern was required in order to stay within the time and cost constraints of the Phase 1 research.

The prototype sensors were then tested in an Accelerated Atmospheric Corrosion Test Chamber constructed especially for that project. This chamber was modeled after one described in the literature [2]. Aluminum, zinc and steel sensors were tested to the end of their useful life which was defined as being an open circuit on the electrical resistance measurement. Tests were discontinued on the copper sensor after 30 days exposure in the chamber. In practice, the actual useful life of a sensor will be determined by the natural corrosion rate of the material itself, the foil thickness and the geometry of the trace.

Weight loss panels were exposed concurrently with the prototype sensors. One set of panels was removed after 15 days, the other after 30 days. Readings were taken from the sensors each work day. The use of concurrent exposures of both types of specimens permitted direct comparisons to be made of the corrosion rates as determined by each of the specimen types. Instrument problems prevented the collection of LPR test data. However, subsequent testing showed that good agreement exists on corrosion data obtained by all three test methods: weight loss, electrical resistance and linear polarization resistance [3].

One of the findings of the Phase 1 project was that sensors made of steel were significantly more sensitive than those made of copper, aluminum or zinc [1]. This suggested that steel element sensors could be adapted to serve as corrosion detectors in environments considerably more benign than those originally envisioned for these sensors. The output of the sensors, when used as corrosion detectors, must be considered qualitative in nature since only steel is being used as the sensing element. In order for the sensors to be quantitative, the sensing element must be made of the same metal as the structure of interest.

As pointed out earlier, sensors of our design concurrently use two common methods of determining corrosion activity: Electrical Resistance (ER) which measures cumulative corrosion loss and Linear Polarization Resistance (LPR) which measures instantaneous corrosion rate. Dual measuring capability is a unique feature of these sensors and would prove particularly advantageous when they are used as corrosion detectors in nominally "dry" areas such as ordinance storage sites or electronic enclosures. In the ER mode, the sensor will record all corrosion which occurs including normal indoor atmospheric oxidation. In the LPR mode, the sensors will fully respond when the surface is wet, such as would occur if atmospheric moisture condensation has occurred, and will partially respond when the humidity is high enough to permit electrochemical activity.

It is well known in the field of corrosion that the presence of a surface film of moisture can accelerate corrosion by an order of magnitude or greater over that which would occur in the absence of the surface film. The practical implications of the sensor's ability to discern between condensing and noncondensing conditions is that it can be used to determine the integrity of hermetically sealed or otherwise intentionally dry environments.

In a continuously wet environment, cumulative corrosion as measured by both the LPR and ER modes should be essentially the same. In a low humidity environment, the LPR reading will be zero while the ER reading would be a record of the normal atmospheric oxidation which has occurred, including that which had occurred under conditions of high humidity but no condensation. Steel is a particularly good detector metal for this application. Recent European work has shown that the instantaneous atmospheric corrosion rate of steel is proportional to the relative humidity (RH) [4]. Over RH ranges of 55 - 95 percent, a semiquantitative power law relationship exists between these two quantities.

Any reading from the sensor in the LPR mode would be indicative of high humidity or condensing conditions and therefore necessary corrective actions should be immediately initiated. High readings in the ER mode only would be indicative of prior, but not present, existence of corrosive conditions. This would also warrant investigation.

It is conceivable that some semiquantitative information can be derived from the sensor when it is used as a detector. The ratio between the corrosion rates measured by the LPR and ER modes would be proportional to the amount of time the surface was wet, but this relationship certainly will not be linear. There will also be a rough correlation between the corrosion rate of the steel element of the sensor and that which would be exhibited by other metals in the same environment. These correlations must be determined empirically and in specific environments.

Sensor Design Refinement

The first part of the present study was devoted to refining the design of the sensor from that shown in Figure 1. Refinement included both an overall size reduction as well as optimizing details of the various features of the trace. Separate working patterns for the ER and LPR portions of the sensor were prepared so that they could be evaluated independently. A composite pattern combining the features of the preferred ER and LPR working patterns would be prepared as the final pattern. Concurrently, an electronic consultant with prior experience in the design of linear circuits for corrosion instrumentation was brought in to the project. The consultant was asked to review the previous work and to comment on the proposed approach.

The consultant recommended [5] that the ER section not be located at the midpoint of the LPR trace as was done in the earlier designs (Figure 1). The applied potential levels necessary to query the ER part could be one or two orders of magnitude greater than those being applied to the LPR part and thus could affect the LPR readings. Alternatively, reducing the ER query voltage to the point where it would not affect the LPR

readings would make ER signal capture extremely difficult. In addition, a microprocessor would likely be required to switch between the two modes.

Consequently, the final pattern consists of four distinct traces in close proximity: two representing the two LPR electrodes and two representing the two ER electrodes. Each mode operates independently of the other, but the key feature of the sensor, that of having two independent means of measuring corrosion activity on a miniature sensor fabricated from a single piece of material, is retained. This pattern is more fully described in Section 3, Final Sensor Design. The remainder of this section will provide a summary of the design refinement experiments done as part of Task 2 of this project. More detailed coverage of this work is contained in Interim Report No. 2 [6].

Working Patterns - Figure 2a shows pattern A which was designed to evaluate the effect of aspect ratio (trace width:trace thickness) on the response of the ER portion of the sensor. The flexibility of the photofabrication process allowed this design, which is actually three specimens in one. When the pattern is made in 1-mil foil, it can be terminated at pads S and C to provide an ER sensor with a 20:1 aspect ratio and a bulk resistance of about 0.8 ohms. It can also be terminated at pads L and C to provide an ER sensor with the same aspect ratio but with a bulk resistance six times as high. Finally, the same pattern produced from 6-mil foil and terminated at pads L and C provides a sensor which also has a 0.8 ohm bulk resistance but an aspect ratio of only 3.3:1.

Variables evaluated on the LPR sensor were trace width, gap width and exposed area. Three patterns were designed: patterns B and C, as shown in Figure 2b, and pattern D, as shown in Figure 2c. By varying the reduction ratio of the original artwork and selective masking of the etched sensor, it was possible to create seven distinct patterns. In each pattern, one variable was changed while the other two were held constant. The test matrix is shown below, where A = exposed area (sq. in.), T = trace width (mils) and G = gap width (mils).

Variable	Pattern (variable value)	Constants
Area	BL (3.0), BL0 (0.3)	G = 15 T = 300
	C (0.12), C0 (0.012)	G = 15 T = 60
	B (0.12), B0 (0.012)	G = 3 T = 60
Gap	B (3), C (15)	T = 60 A = 0.12
	B0 (3), C (15)	T = 60 A = 0.012
Trace	B (60), D (6)	T = 3 A = 0.12

Test Procedure - Previous work on the kinetics of atmospheric corrosion has shown that virtually all the corrosion activity occurs during periods when the surface is covered by an electrolyte. The actual rate of corrosion during the active periods is dependent on the composition of the electrolyte. Thus, attempts to develop accelerated atmospheric corrosion tests have focused on speeding up the frequency of wet/dry cycles and adjusting the composition of the electrolyte used for the wet cycles to that of the atmosphere of interest [1], [2].

In this program, the concern was to optimize the response of the sensor during the wet periods. Studies of actual corrosion product films and the changes they undergo during the dry-down periods was of secondary concern. For this reason, all optimization testing was conducted in a continuously wet environment, i.e., tank testing. This eliminated the variable behavior associated with a continuously changing environment and increased the accuracy of sensor-to-sensor comparisons.

Duplicate sensors of each design were tested except for the very large BL and BLO pattern sensors in which only a single specimen was tested. Electrical resistivity was measured using the four-wire method to eliminate lead wire resistance. The LPR specimens were energized with an op-amp based potentiostat originally developed during the previously referenced Navy project [3] and further modified for this project. A schematic of the potentiostat circuit is shown in Figure 3. The sensors were only energized during reading events at which time bias voltages of -5, 0 and +5 mV were sequentially applied. The resulting current at each bias was measured and the data set converted to instantaneous corrosion rate.

The test solution was intended to be a mildly corrosive environment and consisted of distilled water with air bubbling through it. A small quantity of NaOH was added to offset the slight acidity increase which occurred after aeration began. The environment was: T = 14C, pH = 7 - 8, DO = 7 ppm, and Cond. = 25 uS.

The corrosion rate of steel, as measured by weight loss panels, was about 5 mpy in the aerated distilled water. This environment proved to be almost too aggressive for the sensors as the thinner sensors (1 mil) lasted slightly more than a week while the thicker ones lasted the full 28 days of testing.

Results: ER Tests - Sensor thickness loss reported by the ER specimens in distilled water as a function of exposure duration is shown in Figure 4. Weight loss data is included for comparison. AK sensors are the 6-mil foil sensors, ANH sensors are 1-mil foil sensors with the same length as the AK sensors, ANL sensors are 1-mil foil sensors with the same resistance as the AK sensors. (Refer to Figure 2a for the actual pattern.)

Two different data reduction models were used. The results from using the first model, shown in Figure 4a, presumes all the metal loss occurs on the top surface. The results from the second model, shown in Figure 4b, presumes equal metal loss from the top and side walls of the sensor. The equations used are shown in Table 1. While the first model is mathematically simpler, the second is more accurate. The difference between the models is 70 percent on the thick specimens with a 3:1 aspect ratio and only 10 percent on the thin specimens with a 20:1 aspect ratio. The actual specimens are not rectangular in shape, as depicted in Figure 8, but slightly trapezoidal. This is inherent to the photoetching process.

The ER sensors consistently reported higher corrosion losses than the weight loss panels. This is normal for the ER method. The data reduction models presume a uniform loss of metal while in actuality the corroded surface is rough and irregular. The effect is that the measured resistance reflects and reports the lesser amount of metal remaining under the deeper gouges. In contrast, the data reduction method used for weight loss treats metal loss as though it had occurred uniformly over the entire surface. In an extreme case where the ER trace is virtually severed by a single corrosion pit, the ER method would report a loss equal to the trace thickness while the WL method would report hardly any loss. In some applications, the enhanced sensitivity of the ER method would be advantageous.

Results: LPR Tests - The corrosion pattern observed on both the sensors and the weight loss coupons made from the same material was not uniform. It tended to start in several discrete areas and gradually spread over the surface of the specimen. On the LPR specimens, it tended to start along the gap, usually near where the lead wire trace joined the exposed LPR trace, and spread from there. This pattern explains some of the differences observed between the corrosion specimens.

Pattern B (Figure 2b) is the base pattern to which the others are compared. It has two parallel electrodes, 2 inch by 0.06 inch, separated by a 0.003 inch gap. Pattern C is the same as B except that the gap has been increased to 0.015 inch to determine the effect of gap width. Patterns B0 and C0 are the same as B and C respectively except that the electrode length was reduced to 0.2 inch to determine the effect of exposed area. This effect was further determined by patterns BL and BL0. They had the same 0.015 inch gap as pattern C but had exposed areas 25 and 2.5 times as great as pattern C. Pattern D (Figure 2c) has a series of interlocking 0.006 inch finger electrodes; the exposed area and gap width are the same as pattern B. This was used to determine the effect of electrode width.

Duplicate specimens were tested in the passive condition, i.e., they were only biased when readings were made. Bias levels were -5, 0 and +5 mV. Corrosion rates were calculated from the

data obtained from each sensor and the average of the two rates was used for analysis. The data reduction model is shown in Table 2. Figure 5 shows the average instantaneous corrosion rates reported by each group of sensors (pattern) as a function of test duration. Figure 5a groups the data to show the effect of gap width, Figure 5b shows the effect of electrode width, and Figure 5c shows the effect of exposed area.

Sensitivity is increased by reducing the gap width, (Figure 5a). Sensors with a 3-mil gap (B & B0) reported corrosion rates approximately twice those reported by the sensors with a 15-mil gap (C & C0). Reducing the gap width reduces the effect of solution IR drop between the electrodes.

Sensitivity is also increased by reducing the electrode width (Figure 5b: B vs. D). "D" sensors reported corrosion rates approximately triple those reported by the "B" sensors. Reduced IR drop which allows a greater area of the sensor to participate in the corrosion reaction is believed be to part of the explanation of this effect. Also contributing is the difference between the area assumed to be corroding and the area actually corroding, as explained below.

Linear Polarization Resistance indirectly measures the corrosion current, Ic, which is a mass loss rate. Ic is converted to a penetration rate by factoring in the density and the assumed area over which the mass loss is occurring. If the assumed area is smaller than the actual area, then the reported penetration rate will be higher than the actual rate, and vice versa. In this test, it was observed that corrosion started in the gap region and spread over the rest of the surface. Thus, toward the beginning of the test, the area actually losing mass was less than that assumed leading to the sensors reporting lower than actual rates. As the area which was actually corroding increases, so would the reported rates, even if the actual rate stays constant. This effect is shown with all the sensors in Figure 5.

The fineness of pattern D leads to a special case. The assumed area was based on the 6-mil trace width. The effective width of the trace is closer to 10 mils (the width plus twice the 2-mil foil thickness) which would lead to the sensor reporting a rate well in excess of that actually occurring as shown in Figure 5. Since metal was being consumed from the pattern D sensor from both the top and side walls, its service life would be shorter than that of sensors with wider traces where sidewall losses would be negligible. This was in fact, the case. By the 20th day of testing, the pattern D sensors were giving no response while the other sensors were still giving a signal.

Figure 5c shows the effect of electrode size (sensors C0, C, BL0 & BL, all with 0.015-gap width). The smaller the electrode, the higher was the reported corrosion rate. This is consistent with the foregoing explanation of assumed area vs. actual area.

It appears that sensor sensitivity is enhanced by increasing the fineness of the pattern geometry, with pattern D being the most sensitive of the patterns tested. The LPR portion of the final sensor, described in Section 3, is a direct derivative of pattern D. In addition, pattern D sensors were used in the packaging study discussed in the next section.

2.0 PACKAGING TEST RESULTS

This section of the study incorporates three distinct sub-tasks: Cleaning after fabrication, Activation prior to exposure and Packaging for long term storage.

Cleaning

After the photoetching process is complete, the remaining photoresist is removed with a strong solvent such as methyl ethyl ketone (MEK). This task investigated whether a subsequent cleaning procedure was required. Four "B" and "D" pattern sensors were used in this test; the sensors had been stored for approximately 9 months without surface protection and consequently had a light tarnish film. Prior to any cleaning, the sensors were immersed in a tank of aerated tap water and the response was recorded for 15 minutes; this provided a base-line response for each sensor. A 20-mV bias potential was used for all tests and the output logged with a strip chart recorder.

A "B" and a "D" sensor were then cleaned by one of four methods and re-immersed into the tank using the same procedures and equipment as was used to determine the base-line response. The cleaning methods were:

(1) Dip in 50 percent strength Clarke's solution. This is one of the solutions listed in ASTM Specification G1 for cleaning steel specimens for corrosion testing. The full strength solution consists of 20 g Sb_2O_3 and 50 g $SnCl_2$ added to 1 liter HCl. The specimens were dipped for 1 minute at room temperature, which was sufficient to brighten them, rinsed in distilled water and warm-air dried prior to immersing them into the test tank.

(2) Dip in inhibited 10 percent H_2SO_4. This solution is also listed in ASTM Specification G1 for cleaning steel specimens. The inhibitor used was 0.5 g/l 1-Ethylquinolinium iodide and the temperature was 120F (50C). A 1 minute dip was sufficient to brighten them after which they were rinsed in distilled water and warm-air dried prior to immersing them into the test tank.

(3) Swab with ferric chloride. This is the etchant commonly used to photoetch steel. The specimens were swabbed for 1 minute, which brightened them, after which they too were rinsed in distilled water and warm-air dried prior to immersing them into the test tank.

(4) Treat with an industrial rust remover, in this case Chesterton No. 358. This is a 25 percent solution of phosphoric acid inhibited with an organic inhibitor such as 2-butoxyethanol. This solution required 2 minutes to brighten the surface after which the specimens were rinsed in distilled water and warm-air dried prior to immersing them into the test tank.

Figure 6 shows a typical strip chart record, in this case for sensor D-3 before (top) and after (bottom) being swabbed with ferric chloride. The horizontal axis is time, increasing from right to left; the vertical axis is the potentiostat output which is proportional to the instantaneous corrosion rate. A different scale factor was used for the two charts; to compare the lower chart to the upper, values from the lower one must be multiplied by 10.

Data from this experiment seemed to indicate that inhibited sulfuric acid is significantly more effective in producing an active surface than the other three solutions used. Ferric chloride was the second most effective followed by phosphoric acid and hydrochloric acid. Figure 7 shows the sensor's response before and after cleaning in each of the four solutions, note that different vertical scale factors were used on each chart. To allow for direct comparison between cleaning solutions, the data has been replotted in Figure 8 which groups the B and D sensors before and after cleaning. Before cleaning, the response of all the tarnished sensors was quite similar; after cleaning, the ranking of the different cleaning solutions is quite evident. The test with sulfuric acid was repeated with a second D sensor to confirm the apparent increased effectiveness of this cleaning solution.

Subsequent work in this area has shown that sulfuric acid dissolves the adhesive layer holding the etched pattern to the substrate. Since the response of these sensors is, in part, dependent on the area exposed to the environment, it now appears that the heightened response was due to a greater area (top-side and under-side) being exposed to the environment rather than due to the exposed surface being more reactive.

The sensors used in the original cleaning tests were laminated to a rigid GRP substrate to facilitate handling. In the later phase of the work, pattern D sensors laminated to a flexible mylar substrate were used. Disbondment was not noted on GRP-mounted sensors as the trace continues to lie flat against the backing even after the adhesive has dissolved. On mylar-mounted sensors, the slightest flexing of the substrate causes the electrode traces to separate. Since the response of sensors cleaned by the other three methods were somewhat similar to each

other and lower than for sulfuric acid cleaned sensors, it now appears that the cleaning method is not as critical as was originally thought.

Also apparent in Figure 8 is the generally increased sensitivity of pattern D over that of pattern B as discussed in Section 1. Corrosion activity has been reported in terms of measured current which can be approximately converted to actual corrosion rate according to the principals of linear polarization resistance. Under the test conditions used, 1 micro-amp measured current would equate to approximately 0.6 mils per year corrosion rate. These rates should be considered as relative rather than absolute since certain key factors in the conversion, particularly the polarization constant, were estimates rather than experimentally measured quantities.

Activation

Several methods of activating the sensors, i.e., pre-corroding them, were tried to learn whether this would enhance the sensor's response. Pattern D sensors were cleaned in warm 10 percent H2SO4, the method which initially appeared to be the most effective in the earlier cleaning trials. (The delamination problem was not discovered until later). After cleaning, each sensor was tested for 15 minutes in aerated tap water to establish baseline data. Next, the sensors were "pre-rusted" by exposing them to a high humidity environment, distilled water or synthetic seawater. Loose rust was removed and the sensors again tested in aerated tap water for 15 minutes. Results are shown in Figure 9.

The top chart shows the baseline response of the sensors after cleaning but before activation. The three sensors showed good agreement with each other: after an initial peak, they stabilized at a current level of about 15 micro-amps. Applied bias voltage in this test was 10 millivolts. These results are consistent with those from the cleaning trials in which sulfuric acid cleaned D sensors stabilized at a 30-uA current level with a 20 mV applied bias (Figure 8). In these two tests, response current appeared to vary linearly with applied bias voltage. Additional work (Section 4) confirmed this observation.

The lower chart shows the response of the sensors after activation. Sensors activated in either distilled water or high humidity behaved similarly: their initial response appeared to be suppressed but after about 5 minutes the current climbed to the 15-uA level of unactivated sensors. The sensor activated by a saltwater exposure responded the same as the unactivated sensors. Based on this work, there appears to be no advantage to activating the sensors.

Packaging

The efficacy of various packaging schemes and their effect on sensor performance was investigated in this sub-task. It was during the course of this work that the delaminating effect of sulfuric acid was discovered which led to the conclusion that a special cleaning step is not as critical as was originally thought. In fact, degreasing and cleaning the surface with a fine wire brush (stainless steel wires) appears adequate to remove any surface films which may interfere with the sensor's response. This latter method was used to prepare a group of D pattern sensors for the packaging studies.

Duplicate pattern D sensors were packaged with each of four proprietary corrosion inhibiting products following manufacturers directions. Packaged sensors were then stored in a chamber at 80 - 85 percent relative humidity for several months. During the storage period, the sensors were periodically energized at 20 mV and the resultant current recorded. The following products were evaluated:

(1) Chesterton No. 408, a vinyl coating removable by peeling.

(2) Chesterton No. 775, a moisture displacing coating removable by solvent dipping.

(3) Cortec No. 319, a water-based coating incorporating a vapor phase corrosion inhibitor (VCI). It is also water removable.

(4) Cortec No. 127, a polyethylene film containing a vapor phase corrosion inhibitor. The film is made into heat sealable bags; any residual VCI can be removed by an alcohol wipe after opening the bags.

(5) No packaging.

Sensors were energized only at time of measurement with a 20-mV bias, the same procedure used on the prototype sensor electronics, and the resulting current flow was measured. Typically, it takes about 10 seconds for the current flow to stabilize. Measured current vs. time is shown in Figure 10 with each data point representing the average of readings from two sensors. Two products, Ch408 and Ct319 actually aggravated the situation by causing the sensors to corrode faster than the controls. Ctrl1 showed more corrosion activity than Ctrl2 because the former was located in a zone where there was condensation forming on the surface while the latter had no condensation. The remaining two products, Ch775 and Ct127 appeared to offer little or no reduction in corrosion activity compared to that of Ctrl2.

Care should be taken not to draw any adverse conclusions about any of these products based on data from this test. The sensors are extremely sensitive and will detect even small amounts of corrosion activity. In contrast, the products tested were not intended to totally eliminate corrosion but rather hold it to a tolerable level. Since moisture is the greatest single contributor to the corrosion process, the packaging scheme used should be designed to eliminate moisture. The most practical appears to be sealed plastic bags containing a desiccant pack.

3.0 FINAL SENSOR DESIGN

The re-designed corrosion sensor incorporated various features shown to be beneficial in earlier work. The electrical resistance trace (loss measurement) was designed with a high aspect ratio (9:1) to minimize sidewall effects. The linear polarization resistance sensor (rate measurement) was designed with narrow electrodes separated by narrow gaps since earlier work showed both these features enhanced sensitivity. In fact, key dimensions of this part of the sensor are essentially the same as those of the pattern D sensor so data from the pattern D sensor can be used as a predictor of the response of the new combined or dual mode sensor.

The dual mode sensor is photoetched from 1-mil steel foil. It consists of two discrete patterns, main pattern and back pattern. After etching, the main pattern is pressed in to the partially cured adhesive, so as to minimize the area of the exposed side wall, after which the adhesive can be completely cured. This pattern is partially masked during final lamination. The back pattern is completely masked; a double-sided adhesive tape is applied to the underside for attaching the sensor to a surface. The main pattern terminates in four contact pads, the back pattern in two. The layout is such that when the two patterns are assembled to create the sensor, the six contact pads align on 0.1 inch centers. A ribbon cable was soldered to these pads on the prototype sensors; other techniques may be used on follow-on sensors.

Figure 11 shows an overview of the two patterns aligned. Figures 12 - 16 are plan view drawings which show general features of the sensor. All dimensions are in mils. The specific drawings are:

Main Pattern, Figure 12 - This is an overview of the top (partially exposed) side of the sensor showing the contact pad area, the routing of the bus traces from the contact pads to the sensing traces, the relative locations of the two active traces (ERA and LPR), and the mask opening cutout. Bus traces are either 50 or 75 mils wide so as to provide a low resistance pathway. A 75-mil land is provided outside the outer bus traces for bonding the mask. The mask opening is 150 mils larger than

the area to be exposed to make it easier to align during final assembly. The left end of the pattern may be plated to assist in bonding the lead wires.

Detail: ER Active Trace, Figure 13 - This drawing shows design details of the ER active trace which provides a measurable electrical resistance which increases as the thickness of the trace decreases due to corrosion. Its basic feature is a Repeating Element which is an 'S' shaped serpentine, 9 mils wide with a 9 mil gap between adjacent parts of the trace. The overall layout is designed to minimize the voltage difference between adjacent parts of the trace and thus minimize leakage or shorting between them which could occur when the sensor is covered by an electrolyte. The sensor has three rows of serpentines, with each row having 20 Repeating Elements. The 9-mil trace widths are maintained from the origin, E, and point M until they get into the masked area where they are blended into the ERA busses.

Detail: LPR Trace, Figure 14 - This drawing shows design details of the LPR trace which provides for two electrodes which, in service, have a bias voltage impressed between them. The current flow is proportional to the corrosion rate. The basic feature of this pattern is a Repeating Element consisting of two opposed 6-mil wide fingers separated by a 3-mil gap; 41 of these Repeating Elements are arrayed to form the pattern. The electrode fingers extend from a tapered manifold which is 6 mils wide at the far end and gradually thickens to 24 mils at the near end. This 24-mil width is maintained on each manifold until it gets into the masked area where it is blended into the LPR busses.

Back Pattern, Figure 15 - This is an overview of the back (completely masked) side of the sensor showing the relative location of the ER dummy trace, contact pads and the routing of the bus traces from the contact pads to the ER dummy trace. Busses are shown as 50- or 75-mil wide traces so as to provide a low resistance pathway. The ERD1 bus has been extended to provide a 50- to 75-mil trace around the outer perimeter of the sensor. This is to provide some additional stiffness around the perimeter, assist in aligning this trace with the main pattern trace during final assembly, and function as a guard ring. The left end of the pattern may be plated to assist in bonding the lead wires.

Detail: ER Dummy Trace, Figure 16 - This drawing shows design details of this trace which provides a measurable electrical resistance which will remain constant throughout the life of the sensor. It is intended to have the same initial resistance as the ER active trace and serves to compensate for thermal variations in resistivity. Its basic feature is a Repeating Element which is an 'S' shaped serpentine, 9-mils wide with a 9-mil gap between adjacent parts of the trace. The overall layout is designed to minimize the voltage difference between adjacent parts of the trace although this feature is not

as critical as on the ER active trace. The sensor has three rows of serpentines, with each row having 24 Repeating Elements. Every other Element of the right row is connected by a 9-mil shunt to a 24-mil wide bus which in turn blends into the 48-mil wide ERD2 bus. These shunts will be sequentially cut, proceeding in the direction of the arrows, until the resistance of this trace is approximately equal to that of the ERA trace. There is a blank area on the main pattern over the shunts so that nothing critical will be damaged during trimming. To ensure proper alignment, the ERD1 bus must lie directly under the LPR1 and ERA1 busses after final assembly. These traces are interconnected on the electronic circuit board to the power supply common so that they also function as a guard ring.

4.0 ELECTRONIC CIRCUIT DESIGN

Circuit Description

The meter consists of four separate sections: connector cable, battery check circuit, corrosion rate circuit and cumulative loss circuit. Component layout on the circuit board is shown in Figure 17. Figure 18 shows the circuit board trace as viewed from the parts side. The label on the case is shown in Figure 19.

Connector Cable - The following color code is used on the ribbon cable connector:

Color	DB9 pin	Sensor Element
White	5	ER Dummy Trace, Common
Gray	9	ER Dummy Trace, Common
Purple	4	ER Dummy Trace, Signal
Blue	8	ER Active Trace, Common
Green	3	ER Active Trace, Common
Yellow	7	ER Active Trace, Signal
Orange	2	LPR Trace, Signal
Red	6	LPR Trace, Common
Brown	1	LPR Trace, Common

Note: The dual lines used for the common end of the traces are joined at the sensor and at the board end of the cable run. Common traces on the sensor are those which go around the periphery of the sensor.

Battery Check (Figure 20) - Two sets of batteries, each consisting of four AA-size cells, provide a +/- 6 V power supply to the circuit. Only the level of the +6 V set is monitored as these are the ones which are drawn down most heavily. When the battery is checked by pressing the button switch (M4), the battery voltage is placed across a two resistor voltage divide (R8 and R9). A S-8054ALY voltage detector (M1) monitors the

voltage at the divide and lights the green LED (M2) if it is at or above the preset level. The component values used will render a "Battery OK" signal when the battery voltage is above +5.9 V.

Corrosion Rate Circuit (Figure 21) - This circuit is essentially a minipotentiostat. It supplies whatever current is necessary, within the limits of the components, to keep the signal electrode at a preset bias voltage referenced to common. Since the other electrode is at common, the bias voltage is, in effect, applied between the electrodes. A bias voltage in the range 0 to 250 mV is set at trimmer VR4. It has been preset to 20 mV which is within the range of bias potentials for which the resultant current flow bears a linear relationship to instantaneous corrosion rate. Higher bias voltages can be used, but in these cases the resultant current flow will be proportional to the conductivity of the electrolyte covering the sensor rather than the corrosion rate of the sensor electrodes.

An AD711C operational amplifier (U7), set up as a current to voltage converter, supplies current to keep the LPR electrodes at the preset bias voltage. A voltage proportional to this current is generated across R6. An AD524C instrument amplifier (U8) re-references this signal to common before it is sent to the LM3915 display driver (U4). Two additional trimmers, (VR2 and VR3) were added in an attempt to widen the response range of the display driver. Since this did not work as well as hoped, they have been disabled by setting them to their maximum values: VR2 (100k) should be turned fully in the counterclockwise direction, VR3 (1M) should be turned fully in the clockwise direction.

The LM3915 display driver (U4) has a logarithmic scale so that the total response range of the display is just under two orders of magnitude. LED Bar Graphs operating in the dot mode were selected as the display in order to provide for a display which is easily absorbed and interpreted by operating personnel without extensive training in corrosion. It provides data with only one significant digit of accuracy; for monitoring purposes, this is usually adequate. If more precise data is required, the actual applied bias voltage would be measured between U7-pin 2 and common. The current flow, in microamps, would be 4.5 times the voltage (in volts) measured between U8-pin 9 and common.

Corrosion Loss Circuit (Figure 22) - This circuit is a standard resistance bridge of the type used to query many resistance based transducers. Since the resistance of each sensor trace is also affected by temperature, the circuit has been set up to measure the difference in resistance between the traces, thus removing the temperature effect. The active and dummy resistance traces on the sensor form two legs of the bridge, a pair of resistors on the circuit board, R5, form the other two legs. On a new sensor, when the resistance of the active trace equals that of the dummy trace, the voltage drop across both traces would be equal. As the resistance of the

active trace increases due to thinning from corrosion, the voltage drop across the two sensor traces becomes unequal. An AD524C instrument amplifier (U9) senses this inequality and responds with an amplified signal proportional to it.

LM3914 linear display drivers (U5 and U6) activate an LED on the bar graph array which is proportional to the resistance increase of the active trace and hence the loss of thickness of this trace due to corrosion. The display only lights when the resistance difference between the active and dummy traces is between 0 and 20 ohms. If the active trace has a lower resistance than the dummy, as may occasionally happen with a new sensor, the display will not light until corrosion has raised the resistance of the active trace to equal or greater than that of the dummy. A cumulative corrosion loss on the sensor of about a quarter mil will cause an LED dot in the middle of the range to light. When this level of loss is reported, it is safe to assume that serious corrosion damage has likely occurred to electronic parts in the same environment. These parts should be inspected and a new sensor fitted after the parts have been reinstalled.

Electronics Operation

To query the sensor, plug the DB9M connector on the sensor cable in to the DB9F socket on the electronics.

Battery Check - Check the battery level by pushing the black button (M4); if the batteries are fine, a green LED (M2) will light in the hole marked "OK". If no light shows, the batteries are weak and should be replaced. The batteries are accessed by removing the four corner screws on the cover plate. Remove the cover plate and disconnect the lead wires from the battery pack to the circuit board. The unit uses eight AA-size alkaline batteries. Make sure the batteries are inserted correctly; inserting them backwards will burn out some of the integrated circuits.

Corrosion Rate - The corrosion rate on the sensor is checked by pushing and holding the toggle (M3) down. It should be held about 30 seconds for an accurate reading. The upper bars will light if the sensor surface is partially or fully wetted. The middle bars will light if the humidity level near the sensor is high enough to be of concern. The lower bars will light if the atmosphere is not overly corrosive.

Cumulative Loss - Cumulative loss is checked by pushing and holding the toggle (M3) upward. Each succeeding higher bar corresponds to a thickness loss of about 0.025 mils (0.000025 inch) of steel lost from the sensor surface. When a new sensor is queried for the first time, the lowest bar should light. Occasionally due to minor variations among individual sensors, this bar will not light until after a slight amount of corrosion (about 0.010 mils) has occurred.

5.0 SYSTEM RESPONSE

Electrical Resistance

Handbook values for steel resistivity vary from 10 to 20 uOcm. The Electrical Resistance portion of the sensor was characterized using a value of 18 uOcm. Figure 23a shows the sensor resistance as a function of actual thickness (solid line). Actual resistance, R,act, varies nonlinearly with actual thickness, t,act. according to the equation:

$$R,act = P * l / w * t,act \qquad (1)$$

where P = resistivity, l = length and w = width. It is common practice in ER-type monitoring is to linearize the response of a sensor over a certain span, usually one half the thickness of the sensing element. This is done to simplify reporting data generated by these monitors.

The dashed line in Figure 23a shows the sensor resistance linearized on two points, 1 mil and 0.5 mil; it follows an equation of the type:

$$R,lin = A * t,act + B \qquad (2)$$

where R,lin = linearized resistance and A and B are constants. At all points except at the extreme ends of the span, the assumption of linearity will cause the actual sensor thickness to differ from that presumed by the meter. To determine the magnitude of this difference, it is necessary to calculate the predicted thickness, t,pred, based on a linear span:

$$t,pred = P * l / w * R,lin \qquad (3)$$

This is the value which would be reported by meter with a linear driver. Figure 23b shows the predicted thickness from a linear meter (solid) and the actual thickness at that time (dashed) as a function of measured resistance. The gap between the lines is the error caused by this assumption of linearity. The meter will report slightly higher losses than have actually occurred at any given point. Calculated values for the curves in Figure 23 are contained in Table 3.

The display on the meter is a vertical 20 unit LED bar graph operating in dot mode. The lowest LED dot represents t = 1 mil (no loss). Each sequentially higher LED dot corresponds to a resistance increase of about 1 ohm and would represent about a represent a cumulative loss of about a half mil or one half of the sensor starting thickness.

The operation of the circuits was verified by using resistors to model the specimens. A 15-ohm resistor was used to model the dummy trace of the ER sensor. The active trace was modeled with a variable resistor in the range of 15 to 30 ohms

which corresponds to a thickness loss of 0 to 0.5 mils on the sensor. Table 4 contains the data from the verification test. The data is presented as shift points, i.e., the approximate resistance increase which causes a shift from one LED to the next sequential one. Also shown are the approximate thickness losses at these shift points based on the linear model discussed above.

In the present design, the display only lights when the resistance difference between the active and dummy traces is between 0 and 20 ohms. If the active trace has a lower resistance than the dummy, as may occasionally happen with a new sensor, the display will not light until corrosion has raised the resistance of the active trace. If the cumulative corrosion loss on the sensor exceeds about a quarter mil, it is safe to assume that serious corrosion damage has likely occurred to electronic parts in the same environment. These parts should be inspected and a new sensor fitted after the parts have been reinstalled.

Linear Polarization Resistance

Polarization Resistance is defined as the slope of the potential/current density curve in the vicinity of the free corrosion potential. In the following sections, the term is used to refer to the slope of a potential/current curve, i.e. an adjustment was not made for the area of the sensor. Since all the sensors were identical, this mathematical shortcut will not have any effect on results where relative corrosion rates are compared. The area of the sensor must be taken into account when the data is converted to an absolute corrosion rate.

Effect of Bias Level & Electrolyte Resistivity - Two Pattern D sensors (similar LPR trace to the final version) were tested at various bias levels and in solutions with various conductivities (distilled, tap and salt waters). Bias voltages ranged from 0 to 100 mV and it took about a minute after application of the voltage for the current to stabilize. The feedback resistor on the op-amp was 1 k so the relationship between the measured voltage and the response is 1 mV = 1 uA. Any size resistor can be used so long as the signal is high enough to read and low enough not to saturate the op-amp. Based on this work, it appears that the optimum bias voltage should be 20 mV.

Figure 24a shows the sensor response current as a function of applied voltage and electrolyte conductivity. A and C are the two sensors, DW, TW and SW are the electrolytes. This data is re-plotted in Figure 24b to show the average response of sensors A and C as a function of the electrolyte resistivity for various bias levels. The sensor has a direct linear response with the applied bias voltage, Vb, and an inverse linear response with the logarithm of the electrolyte resistivity. This is in line with the expected behavior of these types of sensors.

Effect of Data Reduction Model - Ultimately, the quantity being measured is the corrosion rate which varies inversely as the polarization resistance, Rp, which is defined as dE/dI, i.e., CR = K(1/Rp) where K is a constant accounting for the sensor material and exposed area.

Figure 25 shows 1/Rp as a function of the applied bias, Vb, for three electrolytes: distilled, tap and salt waters. Since one of the two bias voltages used was zero, dE = E so Rp = E/dI. The problem comes with response current; the two electrodes may spontaneously develop a small bias between them due to inhomogeneities in the metal. Therefore, E = 0 is actually an applied bias and hence there could be a response current. To precisely calculate Rp, one should use dI (I @ Vb - I @ 0). However, this would increase the complexity of the circuitry by requiring either a microprocessor or alternate means to store the first reading. Since a goal of this project is to keep the electronics simple, we determined the difference in measured rates which would occur if the erroneous assumption was made that I = 0 at E = 0 so Rp = E/I. It turns out that this creates an error at low bias voltages which decreases as Vb increases. Figure 25 shows 1/Rp using both methods, E/I and E/dI, for three different electrolytes.

The corrosivity of the three test media varies widely and, hence, measured corrosion rates will vary over several orders of magnitude. To facilitate comparison of the data, it has been re-plotted in Figure 26 using the log of the inverse polarization resistance. The average readings of the two sensors rather than their individual readings was used to keep the graph from appearing too busy.

Two things are apparent on examining this figure. First, for applied bias voltages greater than 20 mV, the difference in measured rates between the two modes of data reduction becomes minimal. It is about the same magnitude as the intersensor variation. Second, the error has the effect of reporting a slightly higher corrosion rate (inverse polarization resistance) which is preferable to understating the rate. It appears,therefore, that a functional monitoring unit can be made by setting Vb = 20 mV.

Further verification of the single point technique of doing linear polarization measurements as versus the conventional two point technique was obtained in the course of the Packaging Study discussed in Section 2. During each measurement event, the polarization resistance was measured by biasing the sensor electrodes to plus and minus 10 mV and recording the resulting current flow. As with the single point 20 mV bias, it takes about 10 seconds for the current flow to settle. The inverse polarization resistance is shown as a function of time in Figure 27. The similarity of this curve set with those of Figure 10 is quite apparent.

In Figure 28, data from Figures 10 and 27 are directly compared. For each measurement, the value of 1/Rp, as derived from the two point method, is plotted against the current measured by the single point method. The data lie in close to a straight line with a slope of close to one (0.93). Regression analysis shows the correlation coefficient to be 0.975 (1.0 means perfect correlation). These data demonstrate that the single point technique, used in the dual mode sensor electronic meter, can provide corrosion rate monitoring data equivalent to that obtained with more sophisticated instruments using two point techniques. The range of rates measured in this test was approximately six orders of magnitude and span the range likely to be encountered in service.

Effect of Humidity - It was noted during the Packaging Study (Section 2) that the humidity in the chamber varied over a 10 percentage point spread during the course of the test. In Figure 29, the data for the control sensors has been replotted as a function of relative humidity. Some correlation of the corrosion current with the humidity level is noted.

Meter Correlation - The meter was correlated by replacing the sensor with a variable resistor. A 20-mV bias voltage was placed across the resistor and the resistance varied to determine the LED shift points. The current at these shift points was calculated from Ohm's law. This was treated as a measured current from a sensor which was then sequentially converted to measured current density, polarization resistance, corrosion current and corrosion rate using the procedure shown in Table 2. The following values were used for the constants:

Electrochemical Equivalent: EE = 27.92 (Based on iron going to the double valence oxidation state.)

Polarization Constant: B = 25 mV (An estimate; for a rigorous conversion, this should be experimentally determined.)

Density: 7.86 gm/cc (Handbook value.)

Units Conversion Constant: K = 0.1288 (For adjusting the units from uA/sq cm to mpy)

Area: A = 0.884 sq cm (Calc. from dimensions in Fig. 14)

Applied Bias Voltage: Vb = 20 mV

The results of these calculations are shown in Table 5. On the meter label, the following terms were arbitrarily assigned to steel corrosion rates: High - 4 mpy, Moderate - 1.5 mpy, Low - 0.5 mpy.

6.0 FUTURE WORK

Additional work on the dual mode monitor is being done by Electrochemical Devices, Inc., PO Box 31, Albion, RI 02802. Based on the work to date, several areas for modifications and improvements to both the sensor and the meter have been identified. In addition, three advanced development projects are suggested. One involves using the sensors in conjunction with the newly developed mixed gas environmental chambers to generate quantitative data on various metals in these environments. The others involve extending the technology to develop other types of sensors and experimentally determining the correlation constants used in Table 5.

Sensor

1. Sensor size reductions. The amount of current measured by the LPR part of the meter is dependent in part on corrosion rate and in part on exposed area. Based on the measured currents shown in Table 5, it appears that the LPR trace area could be reduced an additional 50 percent and still produce a sufficiently strong signal for the meter. The ER trace length could be reduce by about a third to a initial resistance of 10 ohms (vs. the present 15 ohms). Furthermore, the area occupied by the ER trace could be significantly lessened by reducing the space between the serpentine loops. Taken together, these three modifications could reduce the overall sensor area by half.

2. Sensor cost reductions. The present sensor is a two layer laminate with a six-wire termination. A design concept exists for a similar sensor on a single layer with a four-wire termination. It represents somewhat of a return to the design shown in Figure 1 but may resolve problems associated with that particular design. A four-wire termination will allow the use of other types of cables and connectors including telephone cable and their associated modular connectors.

Electronics

1. Reduction in power consumption. LED bar graphs consume considerable power during operation. At the time the electronics were designed, LCD bar graphs, which consume much less power, were not generally available except on custom order. Dual LCD bar graphs are now starting to appear in the merchant market. Converting the display to LCD will allow either smaller batteries or longer operation with the same batteries.

2. Alternate power sources. In addition to reducing the power consumption by converting to an LCD display, the power supply can be upgraded by converting to either lithium or re-chargeable batteries. A dual power supply is also possible in which power can be provided from either a commercially available wall-mounted transformer (the type used in many electronics products) or on-board batteries.

3. Display current-time integral In addition to measuring cumulative corrosion by the Electrical Resistance method, one can also independently measure it by integrating the corrosion current measured by the LPR method over time. This presumes that the meter is always on and always connected to the sensor. The method proposed is to use a mercury column coulometer which is a device sometimes used as an elapsed-time meter.

4. Provide signal output to external logger. The signal going to the displays is an analog signal whose strength is proportional to either corrosion rate or cumulative loss. It would be a simple matter to provide a connector or jack on the case so that the meter could be plugged in to an automatic data logging device.

5. Bells and Whistles. Literally! The meter could be designed to alarm at preset rate or loss levels. The alarm could be visual (blinking display or LED), audible (bells and whistles) or some combination thereof.

Advanced Development

1. Quantitative Correlation At the present state of development, the rate meter is semiquantitative as many of the key constants used in data reduction were assumed rather than experimentally measured values. Values of constants B and EE can be experimentally determined by doing a full polarization scan with the sensors. The scan should be done in full immersion using the conventional 3-electrode method as well as in high humidity using the 2-electrode method.

2. Inter-metal Correlation It was originally intended to expose weight loss coupons of several common metals to benign (nonwetted) environments along with the steel sensors in order to develop a correlation between sensor response and behavior of these other materials. This approach proved impractical as weight losses of the more corrosion resistant metals would be too low to be reliably measured.

During the time this research was in progress, others in the field of electronic corrosion were making considerable progress in the design, deployment and use of mixed-gas environmental chambers to simulate indoor corrosion. To date, much of the work done in these chambers has involved exposure of fabricated parts (connectors, contacts, etc.) which were tested before and after exposure to the chamber. A direct and quantitative comparison of

the effects of various atmospheric gas mixes on the corrosion behavior of common metals can now be obtained through the use of these new sensors. Sensors would be manufactured in each of the metals of interest. They would be then concurrently exposed in a mixed gas chamber and the corrosion rate continuously logged.

3. Other Sensor Types. Design concepts exist for a photoetched sensor for measuring fatigue or corrosion fatigue in relatively benign environments. It consists of a fatigue-sensitive element fabricated of the same material as the structure of interest. Potential applications include airframe structures. Since this is a rather novel and untested concept, it would best be done as a two-stage research project. The first would be a small project to prove the feasibility of the concept while the second development stage would only be done if the first stage proved successful.

REFERENCES

[1] "Feasibility of Producing Low Cost Atmospheric Corrosion Sensors"; F. J. Ansuini and R. E. Howe; Final Report under U. S. Air Force Contract No. F33615-83-C-5104; June, 1984.

[2] "An Accelerated Atmospheric Corrosion Test (AACT)"; R. D. Smith; ASTM STP 646; June, 1978.

[3] "Low Cost Seawater Corrosion Sensors"; F. Ansuini; Final Report to Naval Surface Weapons Center, Contract N60921-85-C-0015; October, 1985.

[4] "Effect of Relative Humidity on the Corrosion Kinetics of HSLA and Low Carbon Steel"; S. Tosta and G. Brusco; Corrosion; October, 1984.

[5] Private Communication: Prof. L. McBride, California State University - Chico.

[6] "Optimization of Sensor Geometry"; F. Ansuini; Interim Report under U. S. Air Force Contract No. F33615-85-C-5069; December, 1986.

Table 1 Calculation of Thickness Loss From Resistivity

Model 1 - All metal lost from top surface only.

Approach: Calculate reduced thickness, tr, and subtract from original thickness, to.

$$tc = to - tr = to - \frac{\phi * lo}{wo * R'}$$

where to, lo, wo = original thickness, length, width
tc = thickness of corroded section (thkns loss)
ϕ = resistivity
R' = measured resistance

Model 2 - Metal lost equally from top and side surfaces

Approach: Treat as parallel resistors where Ro = original resistance, Rc = resistance of the corroded portion, Rb = resistance of remaining portion.

$$\frac{1}{Ro} = \frac{1}{Rc} + \frac{1}{Rb} \qquad \frac{1}{Rc} = \frac{1}{Ro} - \frac{1}{Rb}$$

For tc much less than to, the cross section of the corroded area can be approximated by a slab tc thick by wo + 2to thick (See Figure 8). Therefore

$$Rc = \frac{\phi * lo}{tc * (wo + 2to)}$$

$$\frac{1}{Rc} = \frac{tc * (wo + 2to)}{\phi * lo} = \frac{1}{Ro} - \frac{1}{Rb}$$

$$tc = \frac{\phi * lo}{(wo + 2to)} * \frac{1}{Ro} - \frac{1}{Rb}$$

Table 2 *Calculation of Corrosion Rate from Linear Polarization Resistance Measurements*

When a small bias voltage, Vb, is applied between two electrodes, a measureable current, Im, will flow. For bias voltages less than about 20 mV, the current will be directly proportional to the voltage. This proportionality is termed the polarization resistance, Rp, and is inversely proportional to the corrosion current, Ic. The proportionality constant is known as the polarization constant, B:

$$dVb/dIm = Rp = B/Ic \qquad [1]$$

For the case when Im = 0 when Vb = 0, equation [1] reduces to:

$$Vb/Im = Rp = B/Ic \qquad [2]$$

The corrosion current can be directly converted to a mass loss rate, MLR, by means of a proportionality constant known as the Electrochemical Equivilant, EE:

$$MLR = (EE)*(Ic) \qquad [3]$$

Mass loss rate is converted to corrosion rate by accounting for the area, A, and density, D, of the metal:

$$CR = MLR/(A*D) \qquad [4]$$

Substituting equations [2] and [3] into equation [4], the corrosion rate can be expressed in terms of constants or dirctly measurable quantities:

$$CR = K*[(EE)*B*(Im)]/[A*D*(Vb)] \qquad [5]$$

where K is a units adjustment constant. In a given experimental setup, EE, B, A, and D would be constants. Therefore:

$$CR = K'*(Im)/(Vb) \qquad [6]$$

If Im = 0 when Vb = 0, then Vb can also be set as a constant:

$$CR = K''*(Im) \qquad [7]$$

Table 3 Calculated Values for Electrical Resistance Calibration Curves in Figure 22. Resistivity = 18 uOcm

t(act)	R(act)	R(lin)	t(pred)	t(a)-t(p)
0.500	29.921	29.921	0.500	0.000
0.525	28.496	29.173	0.513	0.012
0.550	27.201	28.425	0.526	0.024
0.575	26.018	27.677	0.541	0.034
0.600	24.934	26.929	0.556	0.044
0.625	23.937	26.181	0.571	0.054
0.650	23.016	25.433	0.588	0.062
0.675	22.164	24.685	0.606	0.069
0.700	21.372	23.937	0.625	0.075
0.725	20.635	23.189	0.645	0.080
0.750	19.948	22.441	0.667	0.083
0.775	19.304	21.693	0.690	0.085
0.800	18.701	20.945	0.714	0.086
0.825	18.134	20.197	0.741	0.084
0.850	17.601	19.449	0.769	0.081
0.875	17.098	18.701	0.800	0.075
0.900	16.623	17.953	0.833	0.067
0.925	16.174	17.205	0.870	0.055
0.950	15.748	16.457	0.909	0.041
0.975	15.344	15.709	0.952	0.023
1.000	14.961	14.961	1.000	0.000

Table 4 Approximate resistance increase (ohms) at shift points between LED bars and the corresponding thickness loss.

Shift Point Between Bars	Resistance Increase	Approximate Loss, mils
x - 1	0	0.000
1 - 2	1	0.025
2 - 3	2	0.050
3 - 4	3	0.075
4 - 5	4	0.100
5 - 6	5	0.125
6 - 7	6	0.150
7 - 8	7	0.175
8 - 9	8	0.200
9 - 10	9	0.225
10 - 11	10	0.250
11 - 12	11	0.275
12 - 13	12	0.300
13 - 14	13	0.325
14 - 15	14	0.350
15 - 16	15	0.375
16 - 17	16	0.400
17 - 18	17	0.425
18 - 19	18	0.450
19 - 20	19	0.475
20 - x	20	0.500

Table 5 *Approximate shift points and corresponding calculated steel corrosion rates for LPR meter. Values determined by replacing the sensor with a variable resistor.*

Calculation based on Equation [5] in Table 2 using the following values for the constants:

EE = 27.92 (Fe -- Fe++)
B = 25 mV (estimate)
D = 7.86 g/cc
K = .1288 (units adjustment, uA/sq cm -- mpy)
A = .884 sq.cm. (area/electrode)
Vb = 20 mV (applied bias voltage)

Shift Point	Resist ohms	I,meas uA	i,meas uA/cm2	PolRes ohms	i,cor uA/cm2	CorRate mpy
x - 1	75,000	0.26	0.30	66,270	0.38	0.17
1 - 2	50,000	0.40	0.45	44,180	0.56	0.26
2 - 3	35,000	0.57	0.65	30,930	0.81	0.37
3 - 4	25,000	0.80	0.91	22,090	1.13	0.52
4 - 5	18,000	1.11	1.26	15,910	1.57	0.72
5 - 6	12,000	1.67	1.89	10,600	2.36	1.08
6 - 7	9,000	2.22	2.52	7,950	3.14	1.44
7 - 8	6,400	3.13	3.54	5,660	4.42	2.02
8 - 9	4,400	4.55	5.14	3,890	6.43	2.94
9 - 10	3,100	6.45	7.30	2,740	9.13	4.18
10 - x	1,100	18.18	20.58	970	25.72	11.77

Correlation between lit LED and corrosion rate.

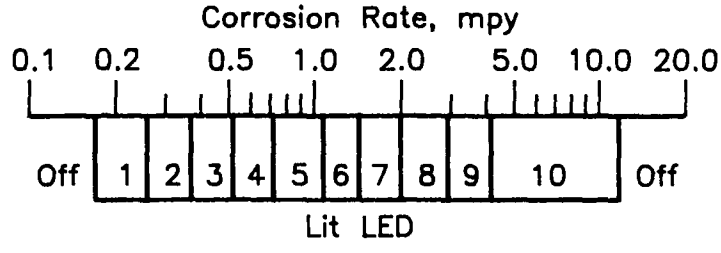

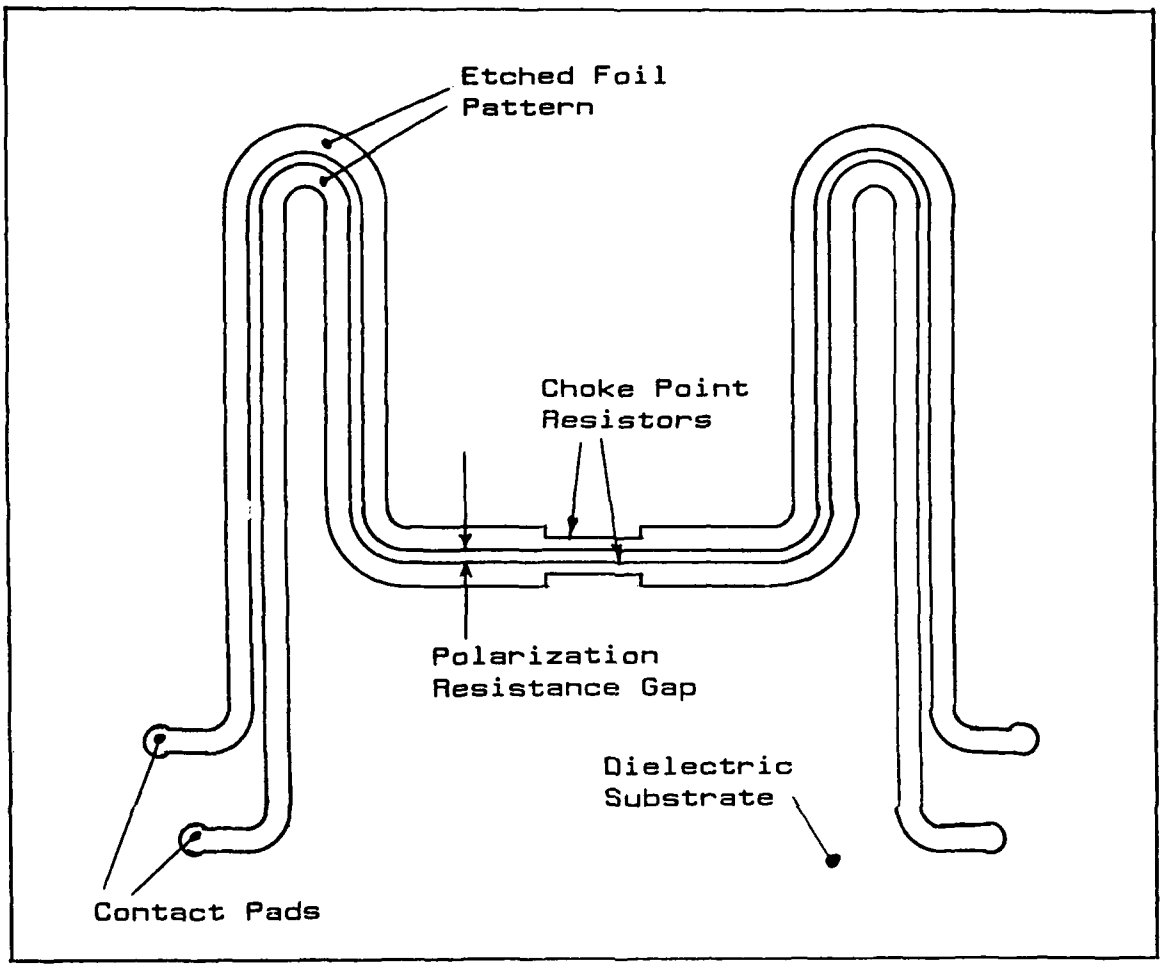

Figure 1. Schematic of sensor design used for proof of concept tests.

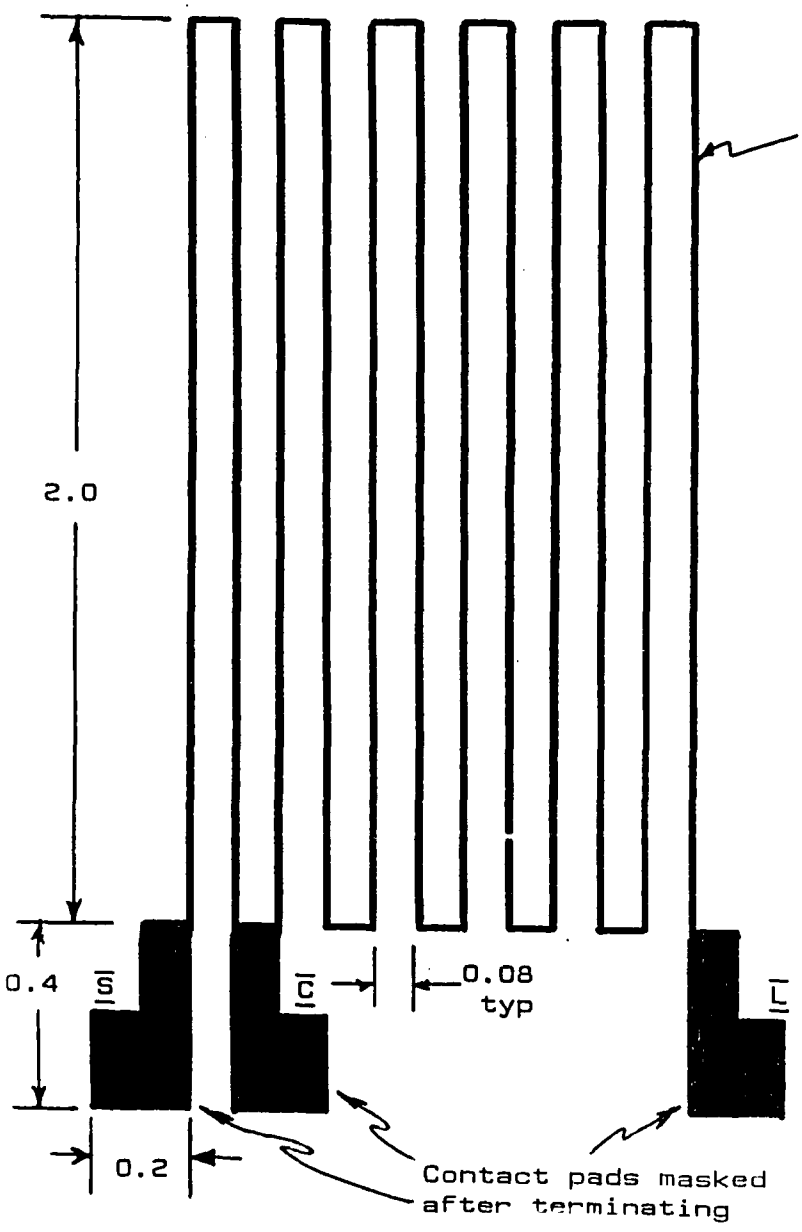

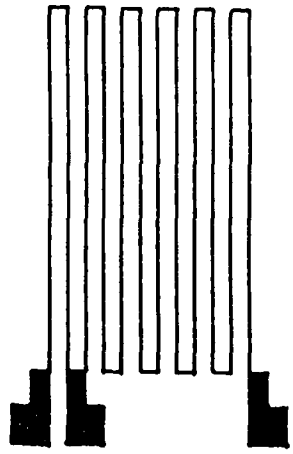

Approximate
Size

Specimen	As	Al
Foil thk. mils	1	6
Trace w, mils	20	20
Aspect ratio w:t	20:1	3.3:1
Elect. contacts	S/C	L/C
Length, in.	4	24
Ohms	0.78	0.78

Figure 2a. Pattern A used for evaluation of aspect ratios on the ER trace.

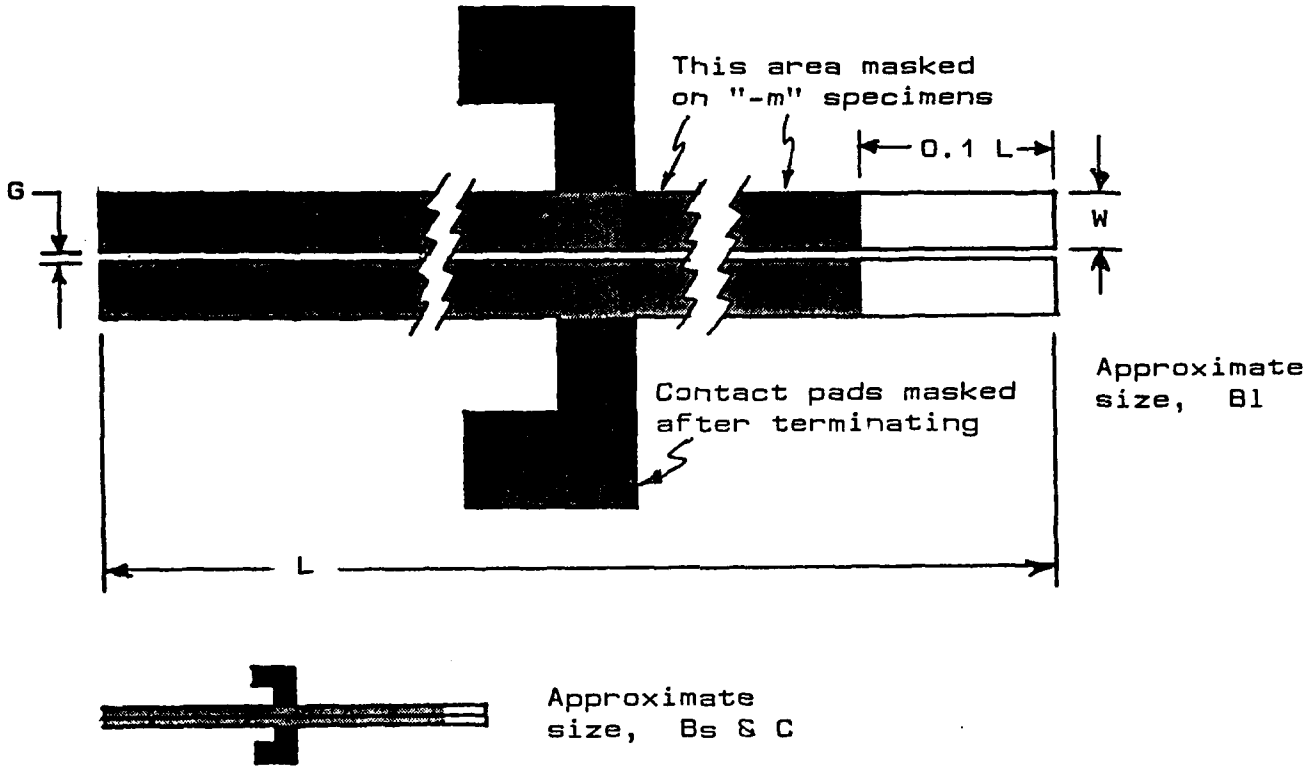

DIMENSION TABLE

Specimen Pattern	Gap G, mils	Width W, mils	Exposed L, in.
B1	15	300	10
B1m	15	300	1
Bs	3	60	2
Bsm	3	60	0.2
C	15	60	2
Cm	15	60	0.2

Figure 2b. *Patterns B and C used for evaluating trace width, gap width and exposed area on the LPR trace.*

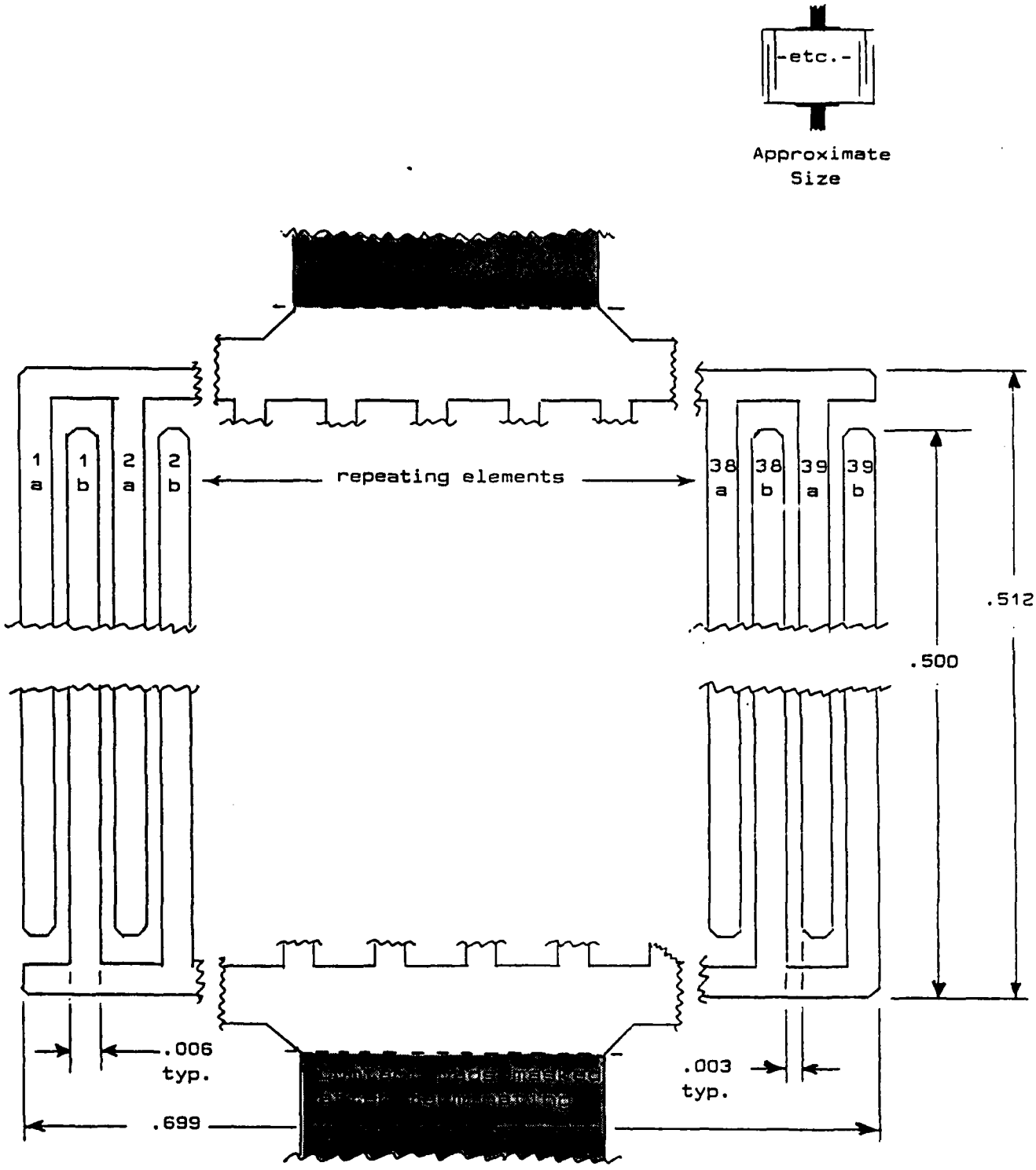

Figure 2c. *Pattern D used to evaluate very fine trace and gap widths on the LPR sensor. A variant of this pattern was used for the LPR trace on the prototype dual mode corrosion sensor.*

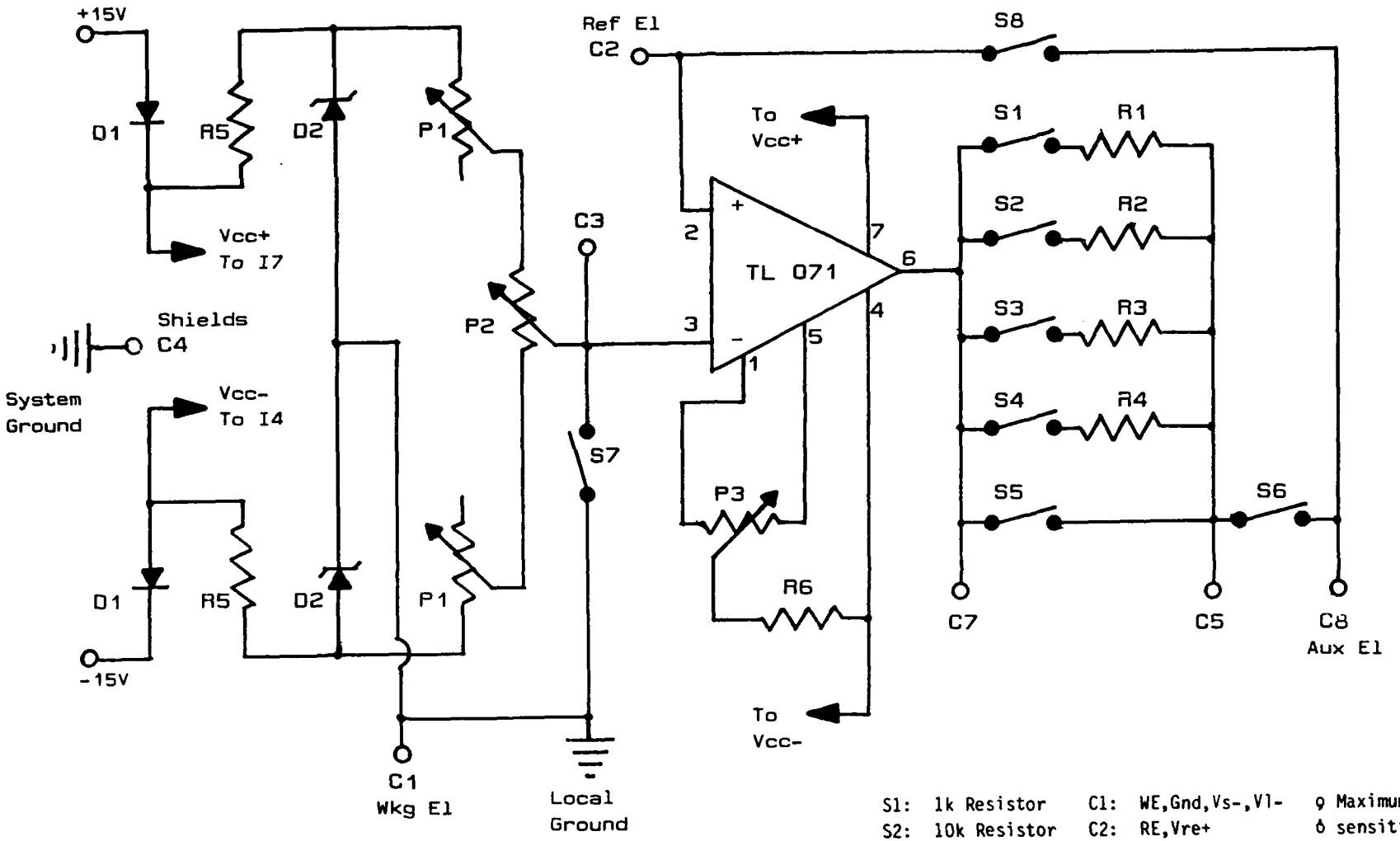

Figure 3. *Schematic of potentiostat circuit used during initial portion of the project. The potentiostat part of the prototype meter circuit is a derivative of this circuit.*

S1:	1k Resistor	C1:	WE,Gnd,Vs-,Vl-	9	Maximum
S2:	10k Resistor	C2:	RE,Vre+	ò	sensitivity
S3:	100k Resistor	C3:	Vs+		
S4:	1Meg Resistor	C4:	Gnd,shields	Top trimmer:	
S5:	Vm Shunt	C5:	Vm-,Amm	CCW incrse +	
S6:	Amm Shunt	C6:	inactive	Bot trimmer:	
S7:	Vs/Gnd Shunt	C7:	Vm+	CW incrse -	
S8:	RE/AE Shunt	C8:	AE,Amm,Vl+		

2 elect. operation: S8 on; 3 elect. operation: S8 off.
Output measured by ammeter: S5 on, S1 - S4 & S6 off.
Outpt meas by voltmtr: S5 off, S6 on, sel range w/ S1-S4.

Data reduction model ignored edge loss effects. (Table 1, Model 1)

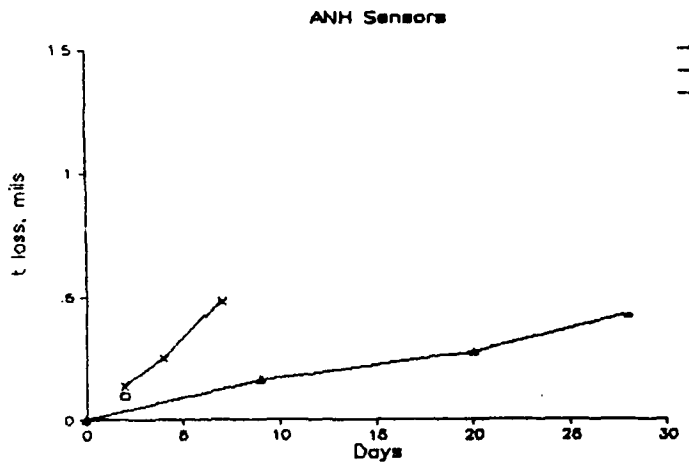

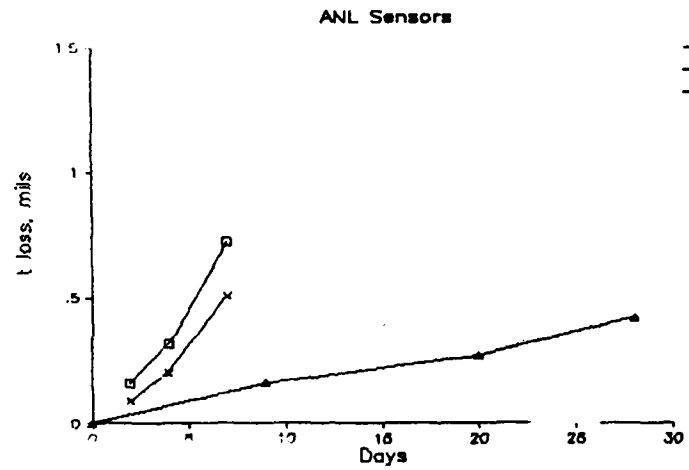

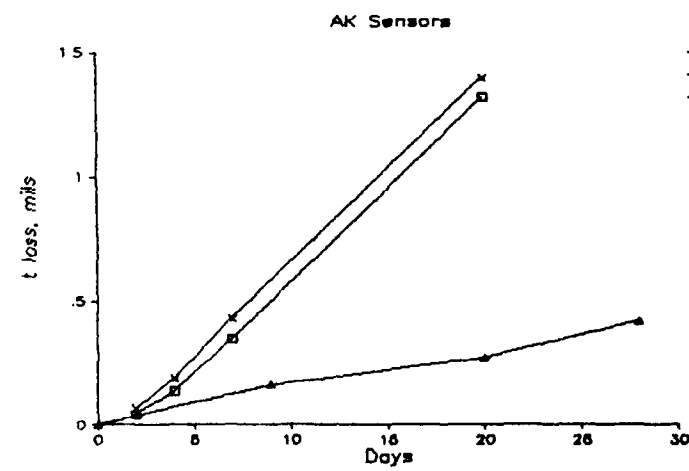

Figure 4a. *Thickness loss as a function of time as reported by the ER sensors*

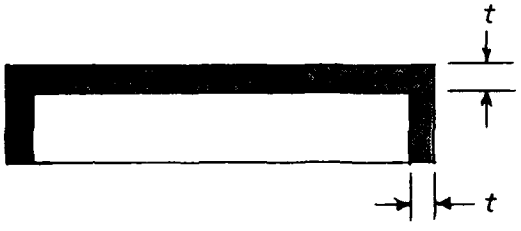

Data reduction model included edge loss effects. (Table 1, Model 2)

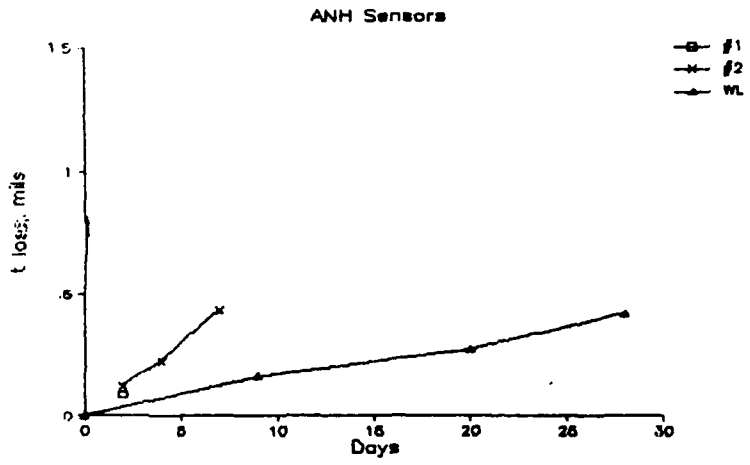

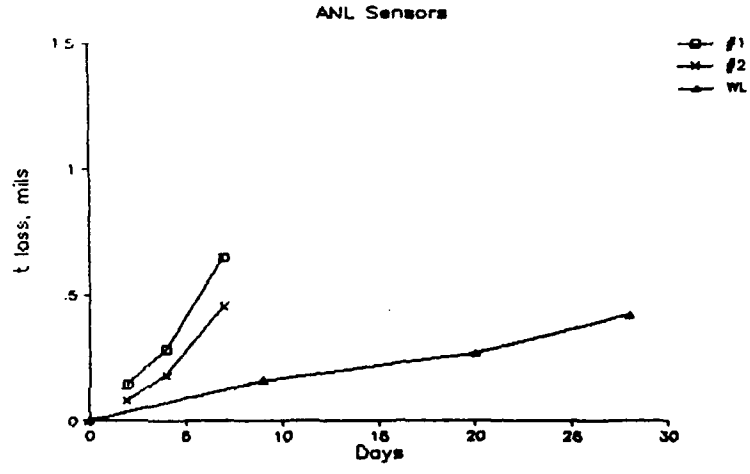

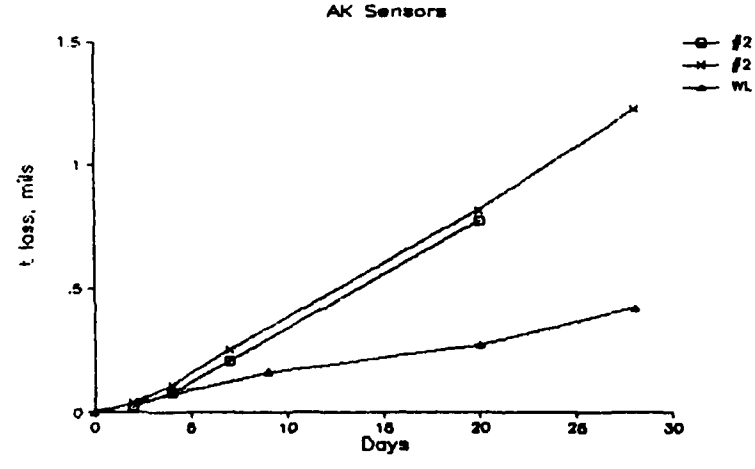

Figure 4b. Thickness loss as a function of time as reported by the ER sensors.

a) Effect of gap width.
Trace width = 60 mils
BO & CO = 0.0774 sq. cm.
B & C = 0.774 sq. cm.

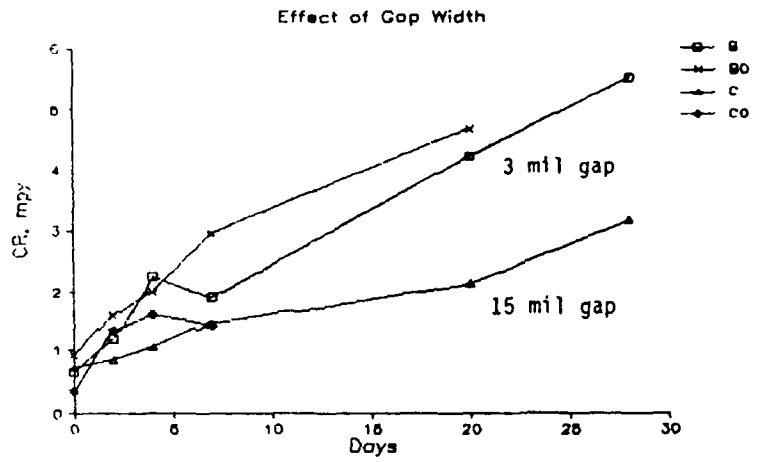

b) Effect of electrode width.
Gap width = 3 mils
Area = 0.774 sq. cm.

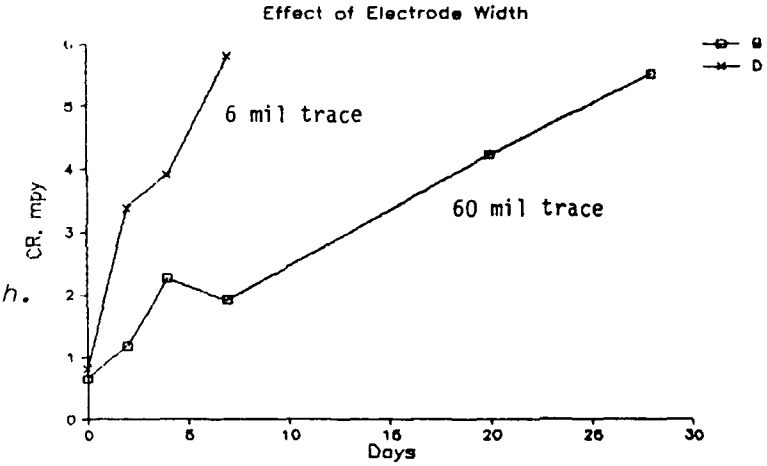

c) Effect of electrode area.
(areas in sq. cm.)
Gap width = 15 mils
BL & BLO = 300 mil trace
C & CO = 60 mil trace

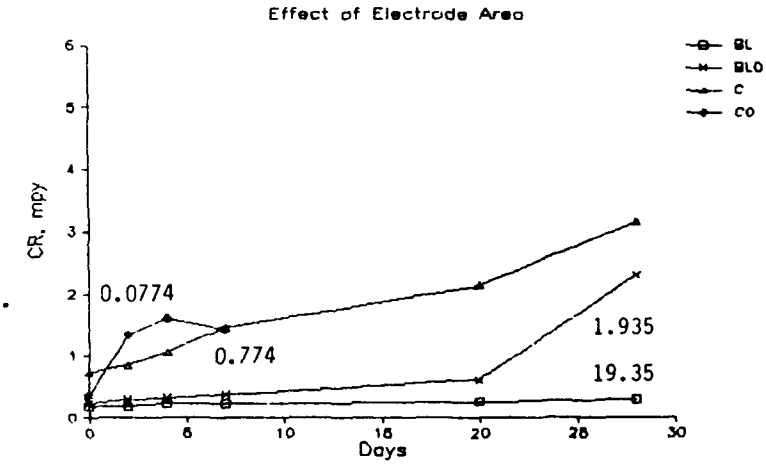

Figure 5. Effect of variations in trace geometry on corrosion rates reported by LPR sensors.

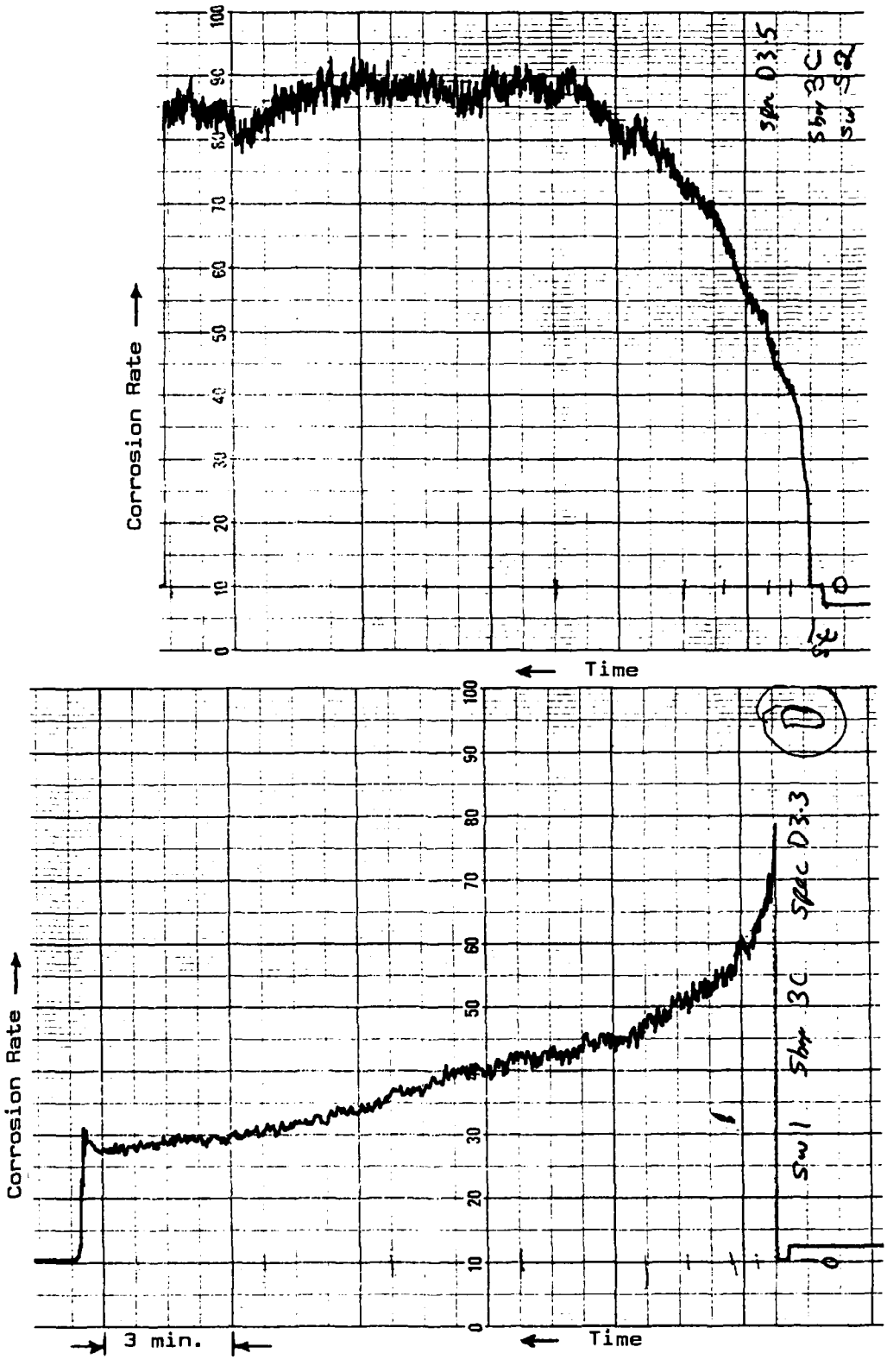

Figure 6. *Typical strip chart record from cleaning tests. Upper chart shows sensor response in aerated tap water before cleaning. Lower chart shows the same sensor after swabbing with ferric chloride etchant. Upper chart vertical scale factor is 10X that of the lower chart.*

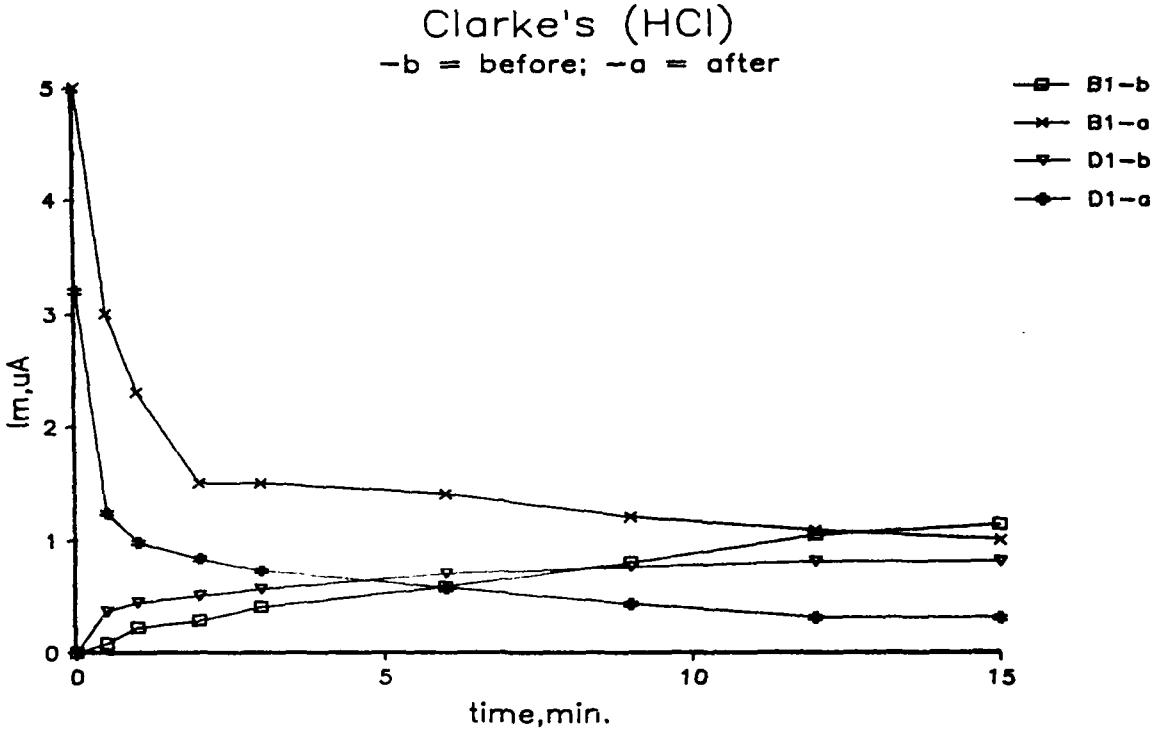

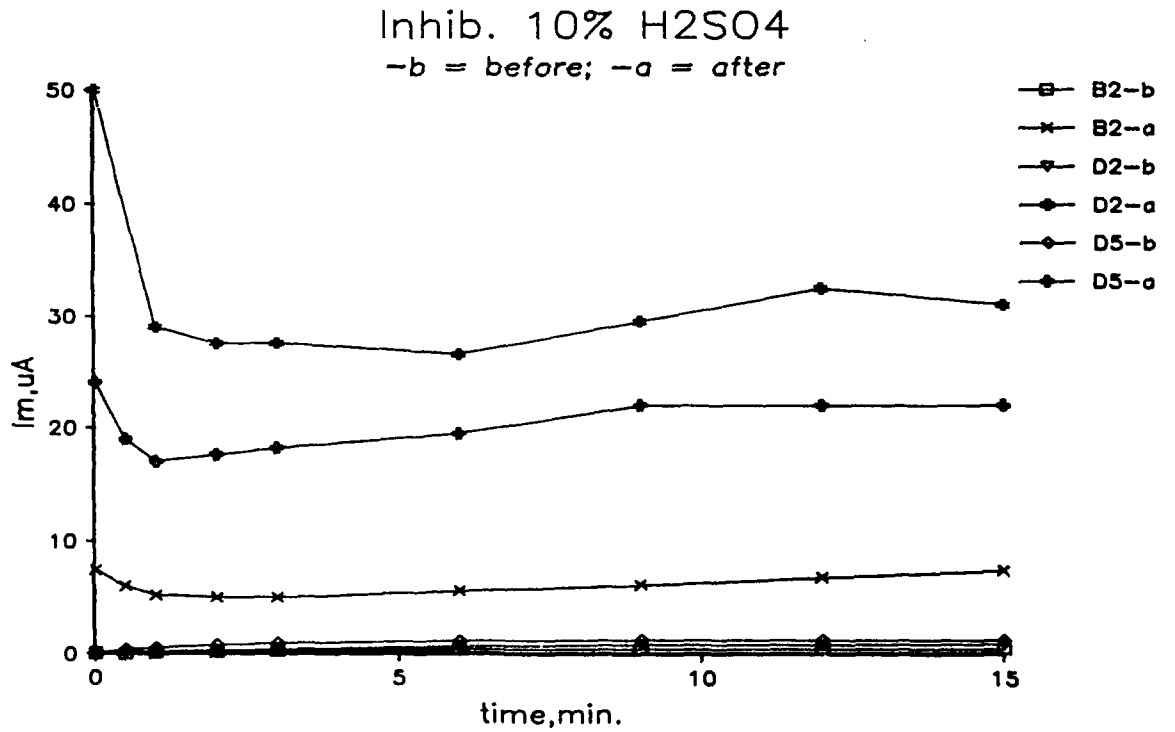

Figure 7. *Effect of different cleaning solutions on sensor response. Charts show the same sensor before and after cleaning. B and D represent the sensor pattern (see Figure 2). Note that different vertical scale factors were used on each chart.*

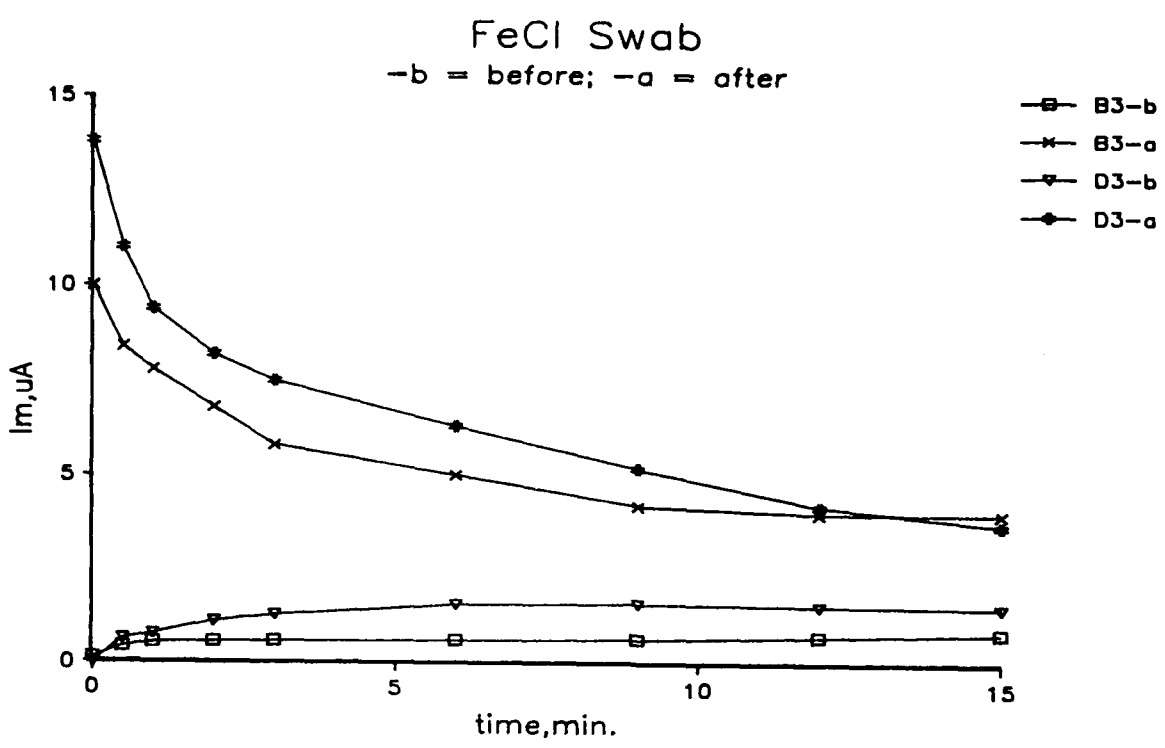

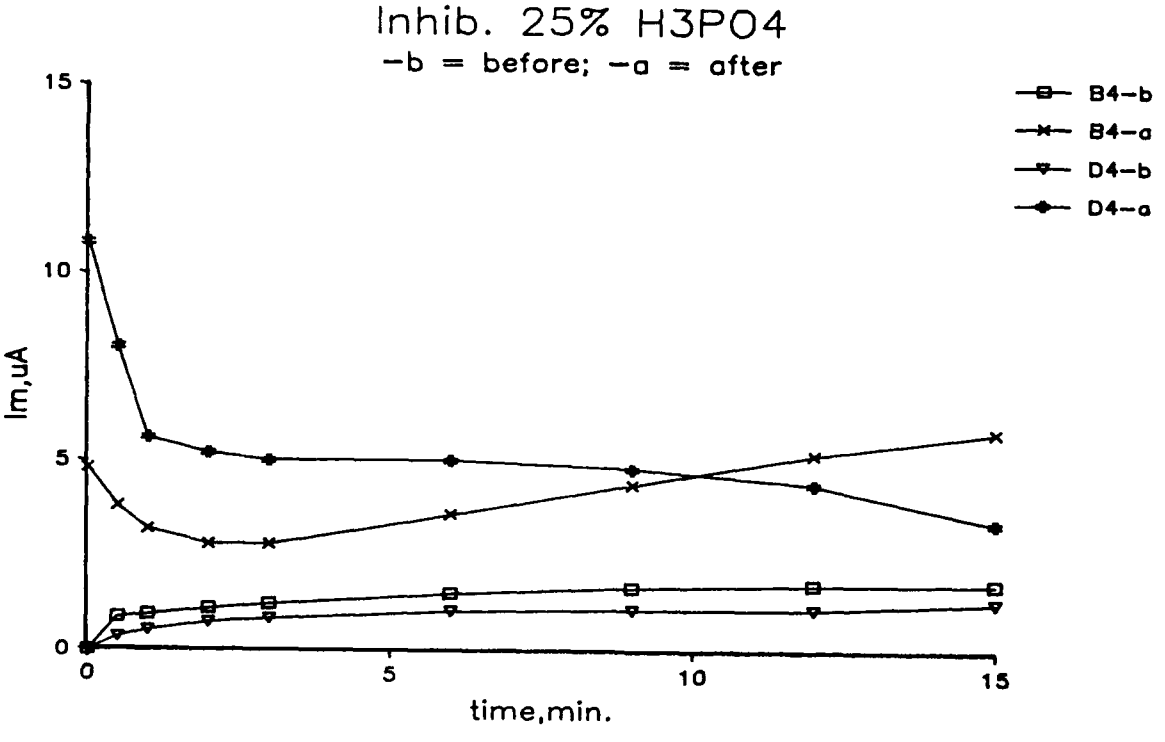

Figure 7. *(continued) Effect of different cleaning solutions on sensor response. Charts show the same sensor before and after cleaning. B and D represent the sensor pattern (see Figure 2). Note that different scale factors were used on each chart.*

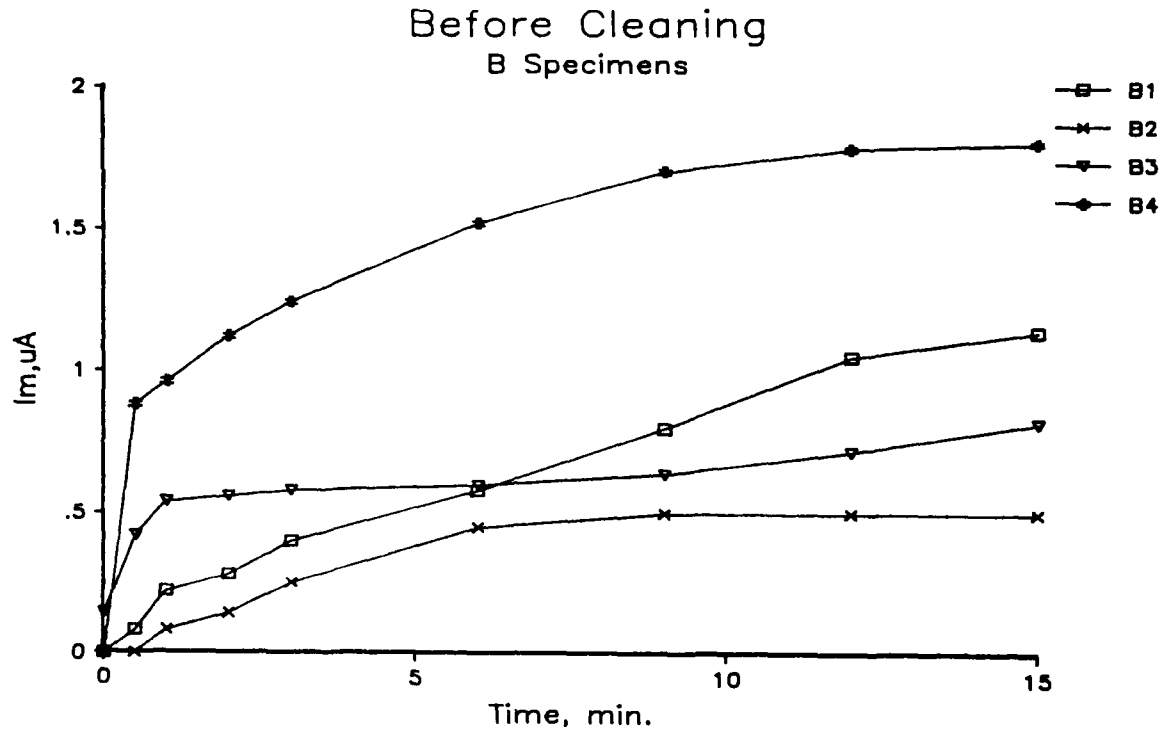

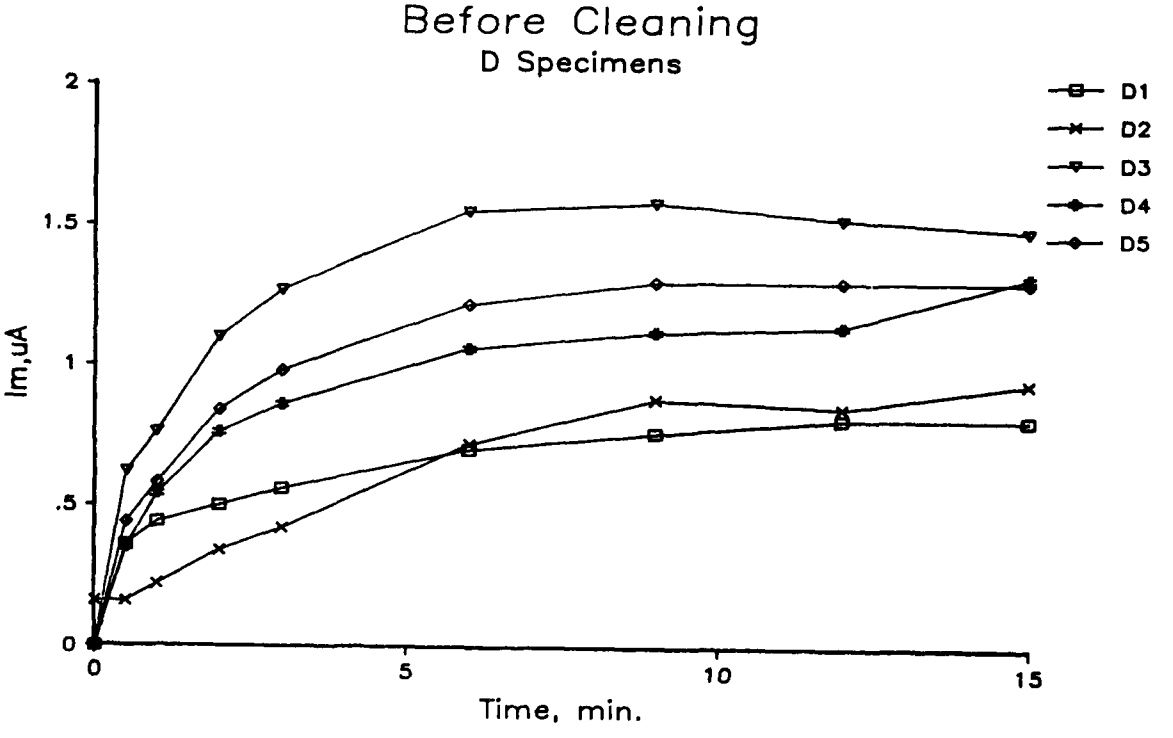

Figure 8. *Response of B and D pattern sensors to aerated tap water before cleaning (as-manufactured).*

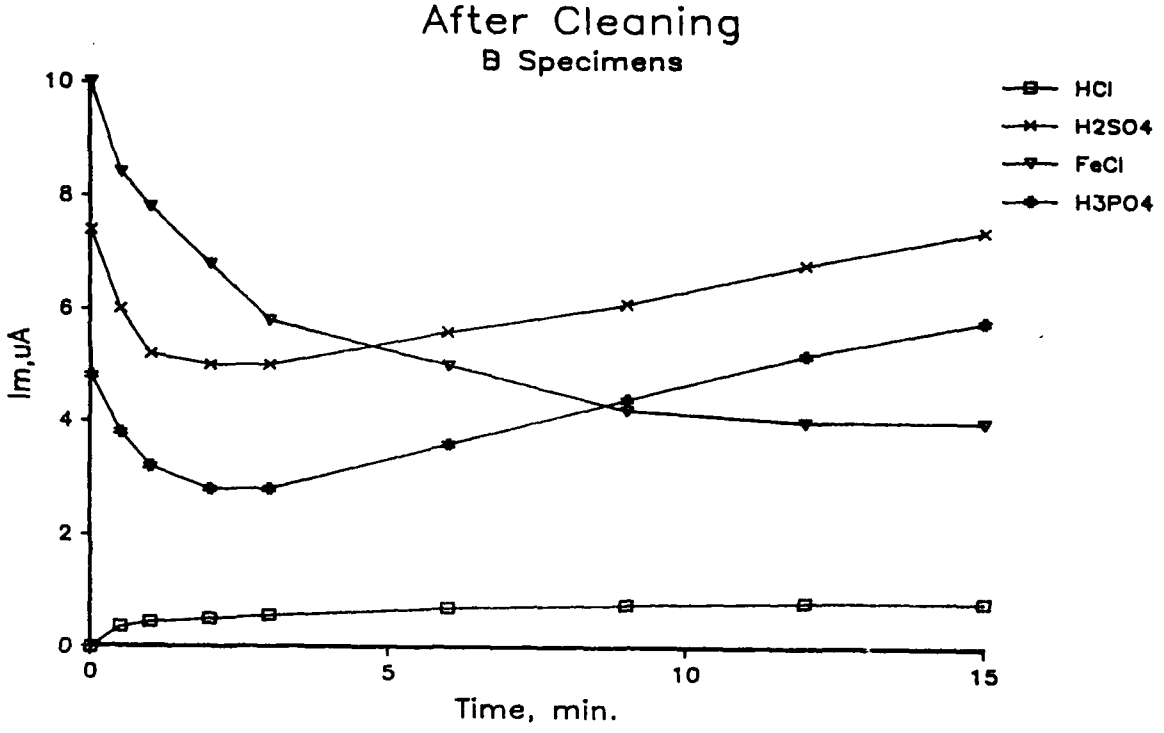

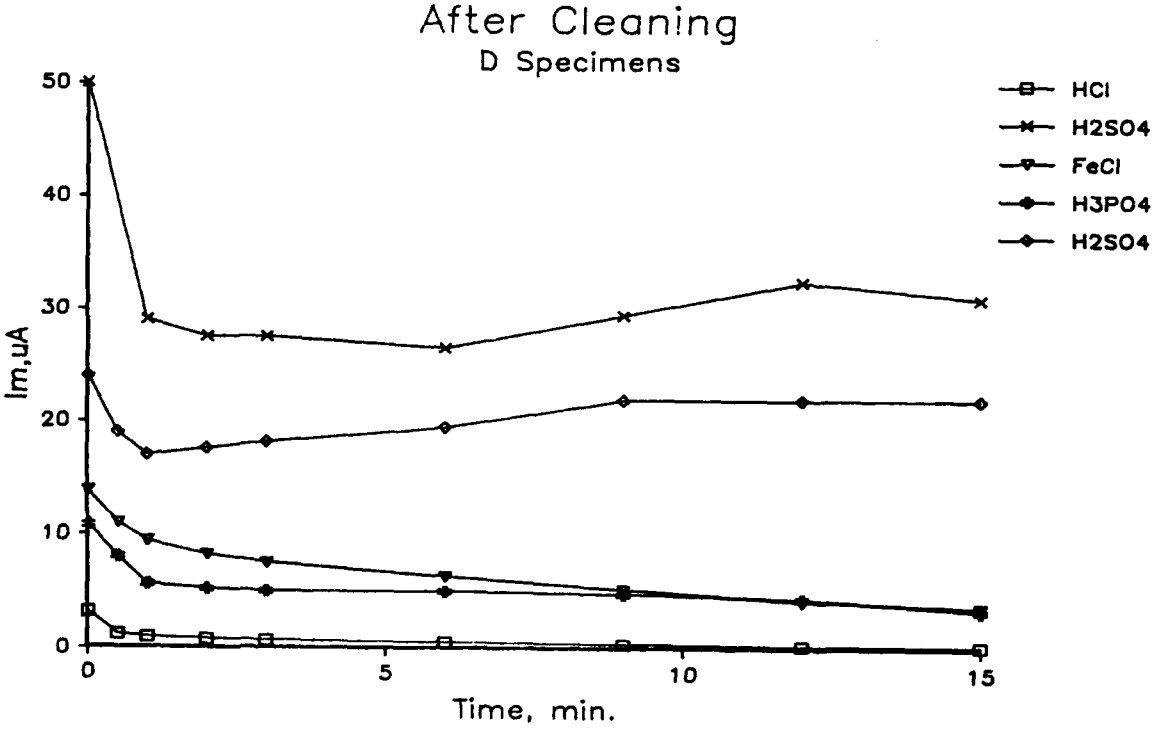

Figure 8. *(continued) Response of B and D pattern sensors to aerated tap water after cleaning by various methods. Note that different scale factors were used in the upper and lower charts. This clearly shows the enhanced sensitivity of the D pattern over that of the B pattern.*

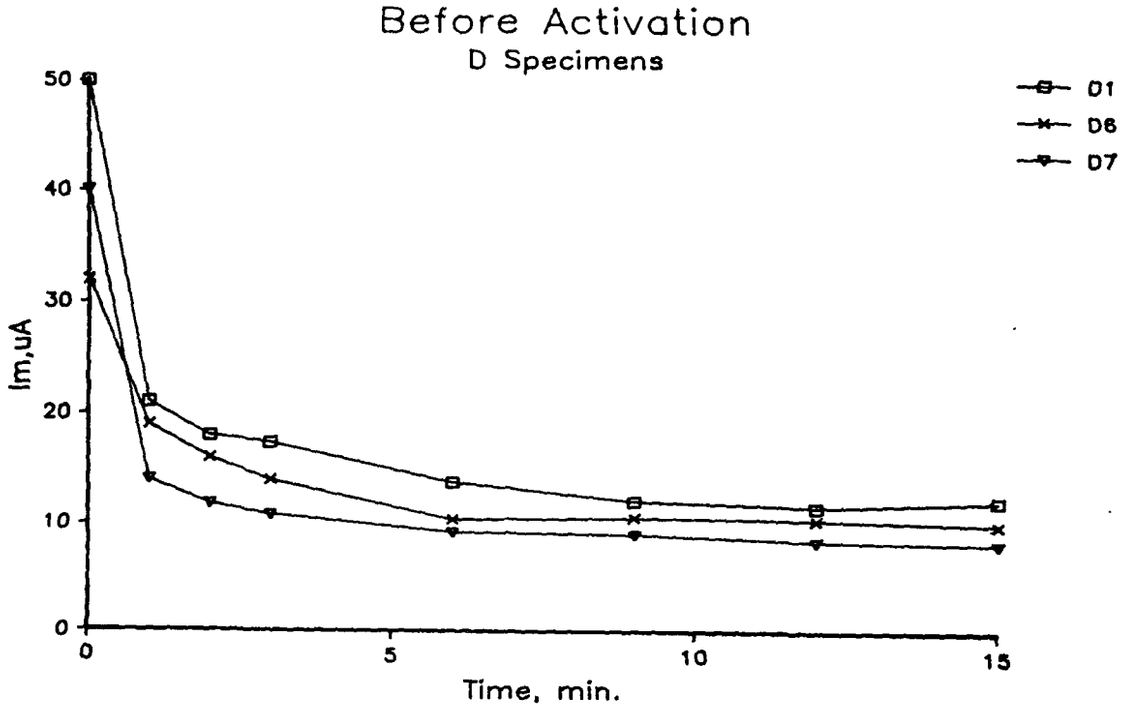

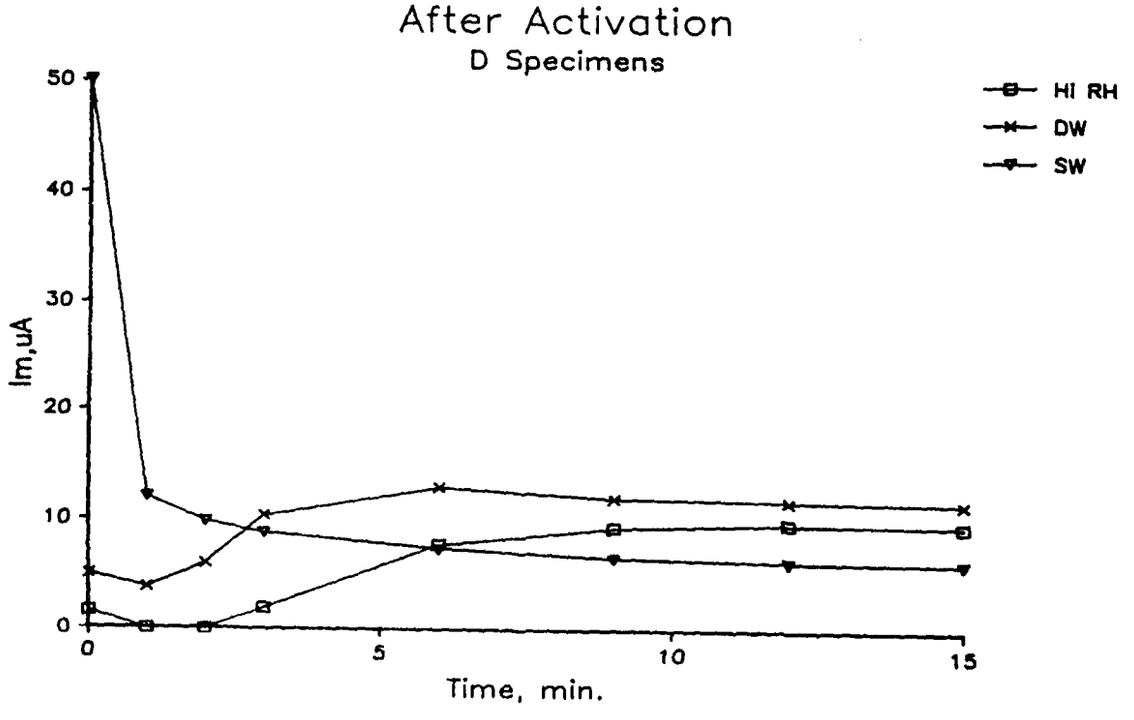

Figure 9. *Response of D pattern sensors in aerated tap water. Upper chart shows the sensors after cleaning in H2SO4. Lower chart shows the same sensors after pre-rusting them in high humidity, distilled water or salt water.*

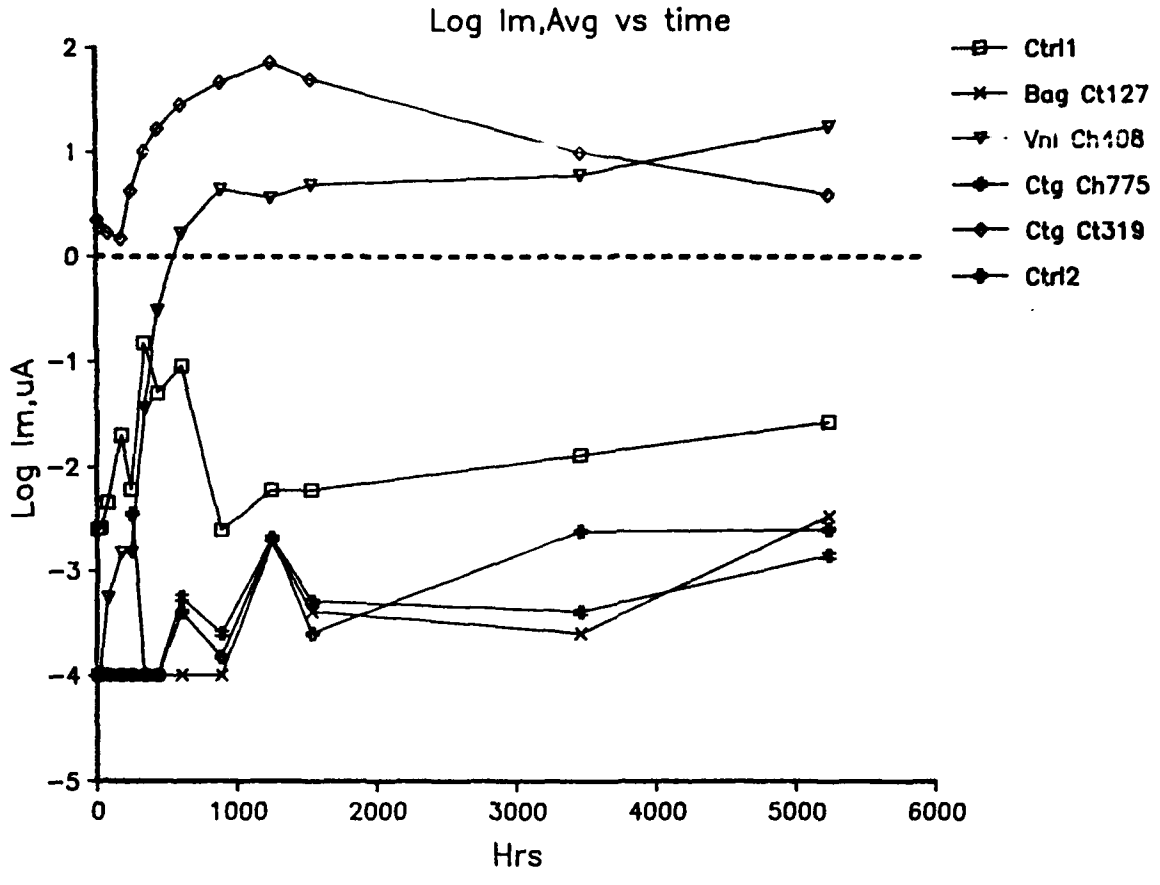

Figure 10. *Response of D pattern sensors in a high humidity (85 percent RH) environment. Sensors were protected by various commercial packaging products as described in the text.*

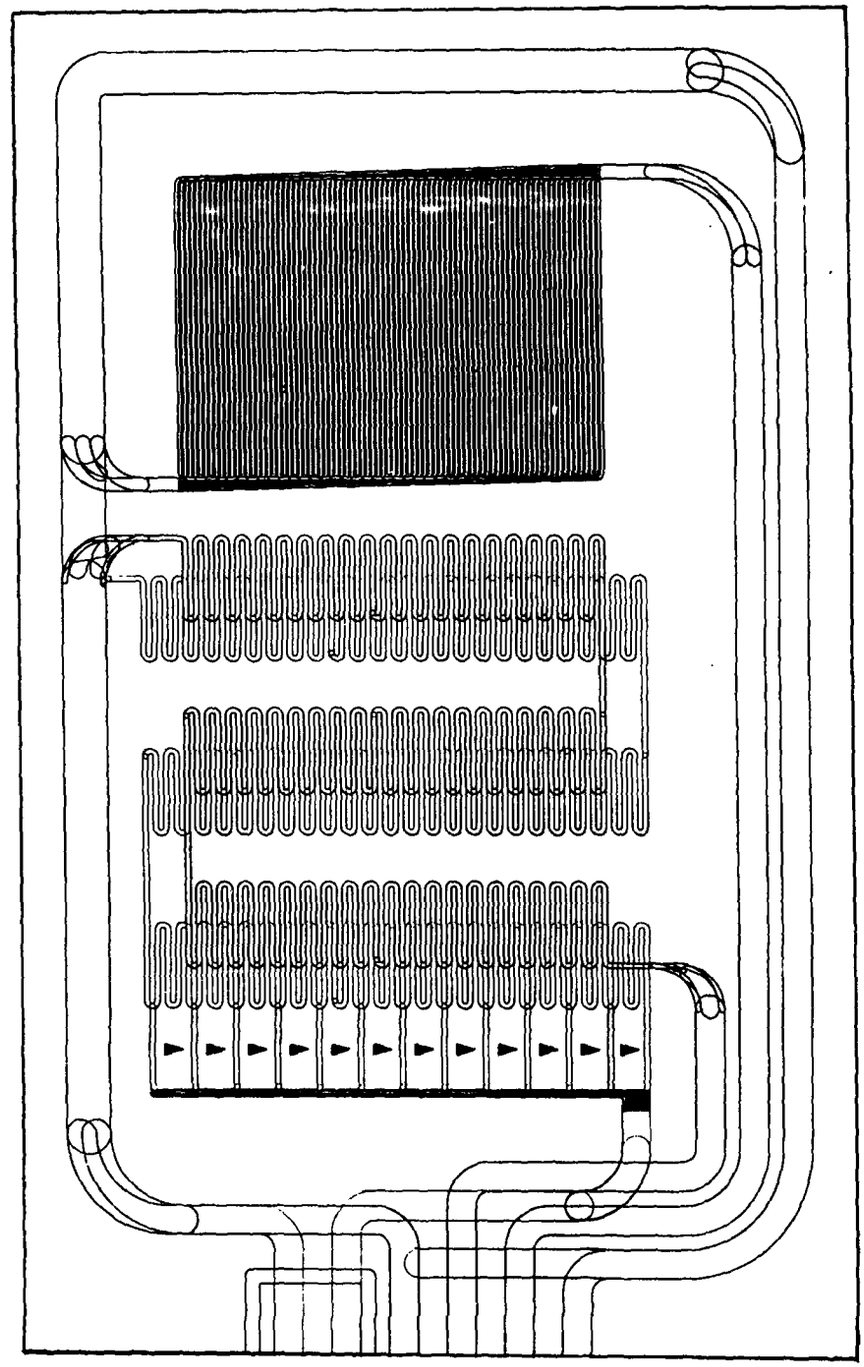

Figure 11. *Overview of the dual mode sensor showing the alignment of the two patterns during assembly.*

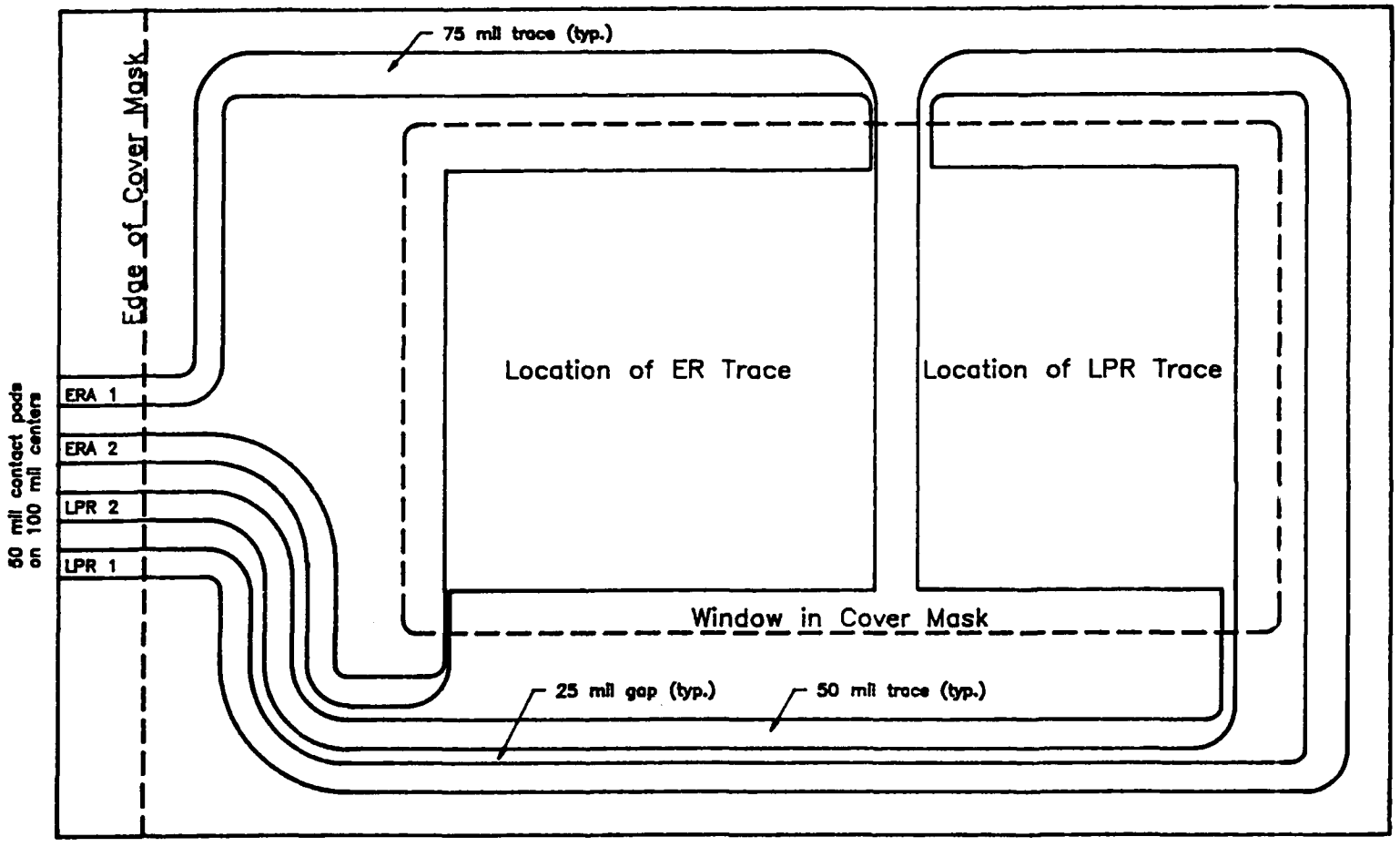

Figure 12. *Main pattern showing bus routing and location of sensing traces. Overall dimensions are approximately 1.4 inches by 2.3 inches.*

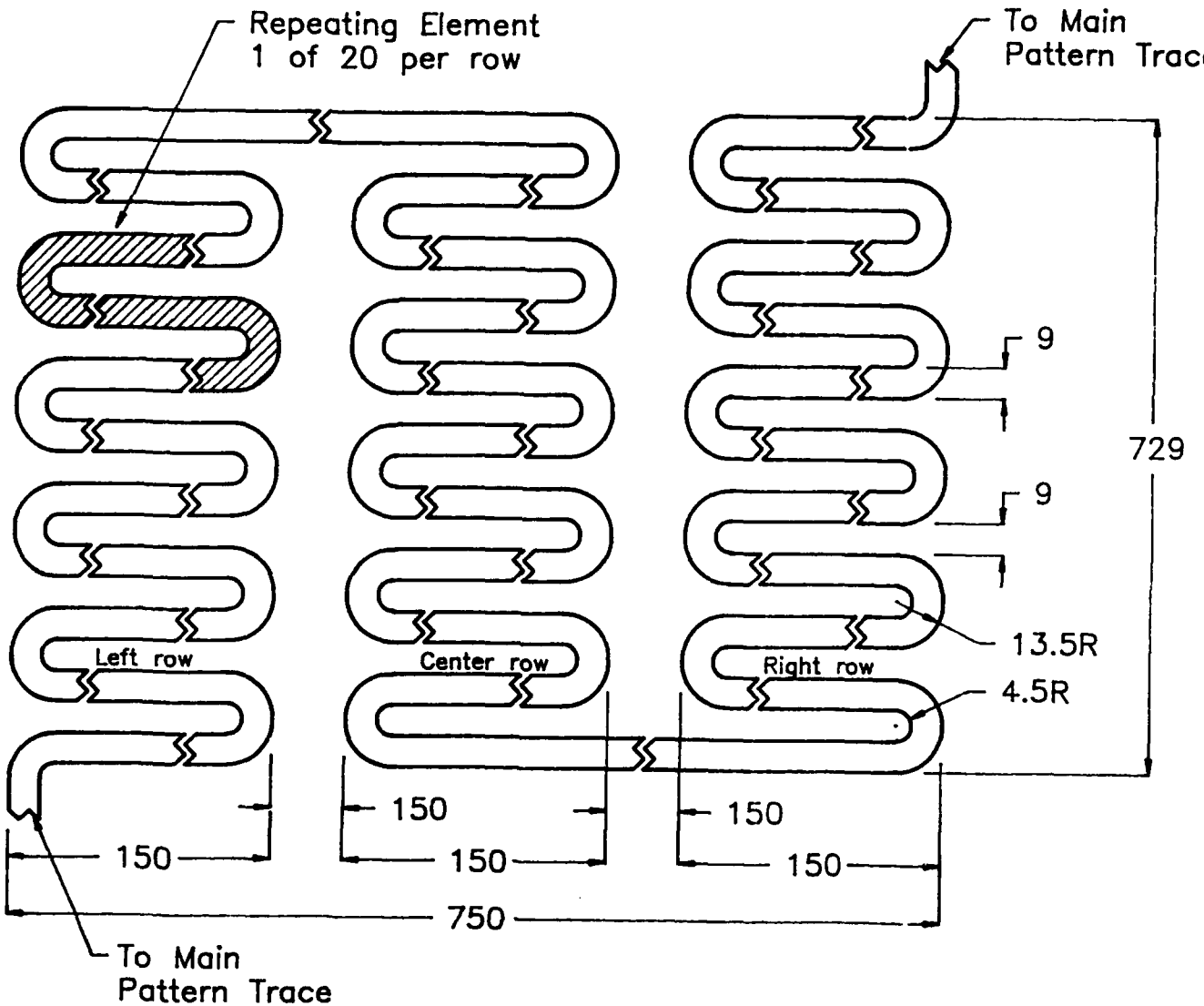

Figure 13. *Detail of Electrical Resistance, Active (ERA) sensing trace. Dimensions shown are in mils (0.001 inch).*

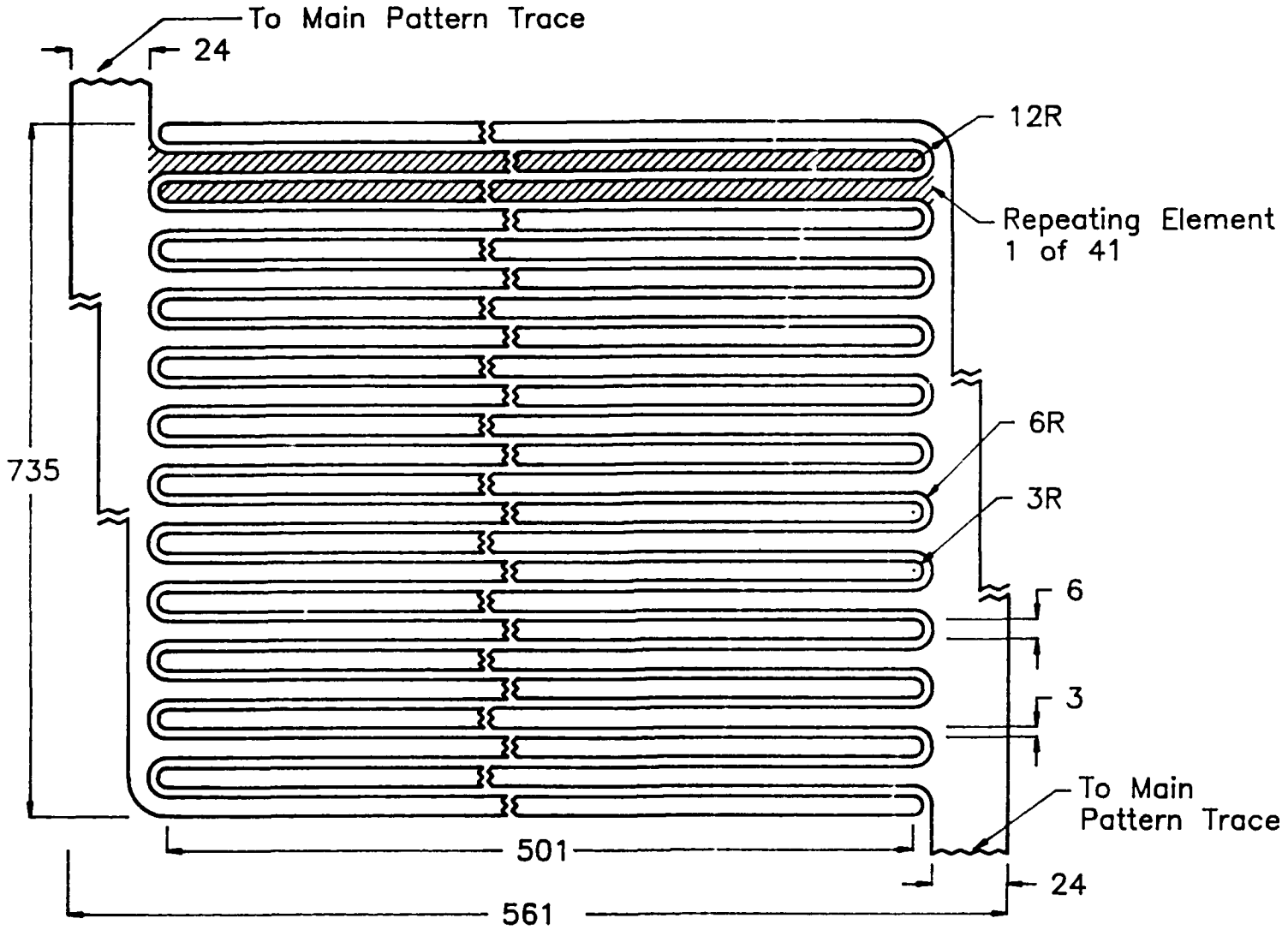

Figure 14. *Details of Linear Polarization Resistance (LPR) sensing trace. Dimensions shown are in mils (0.001 inch).*

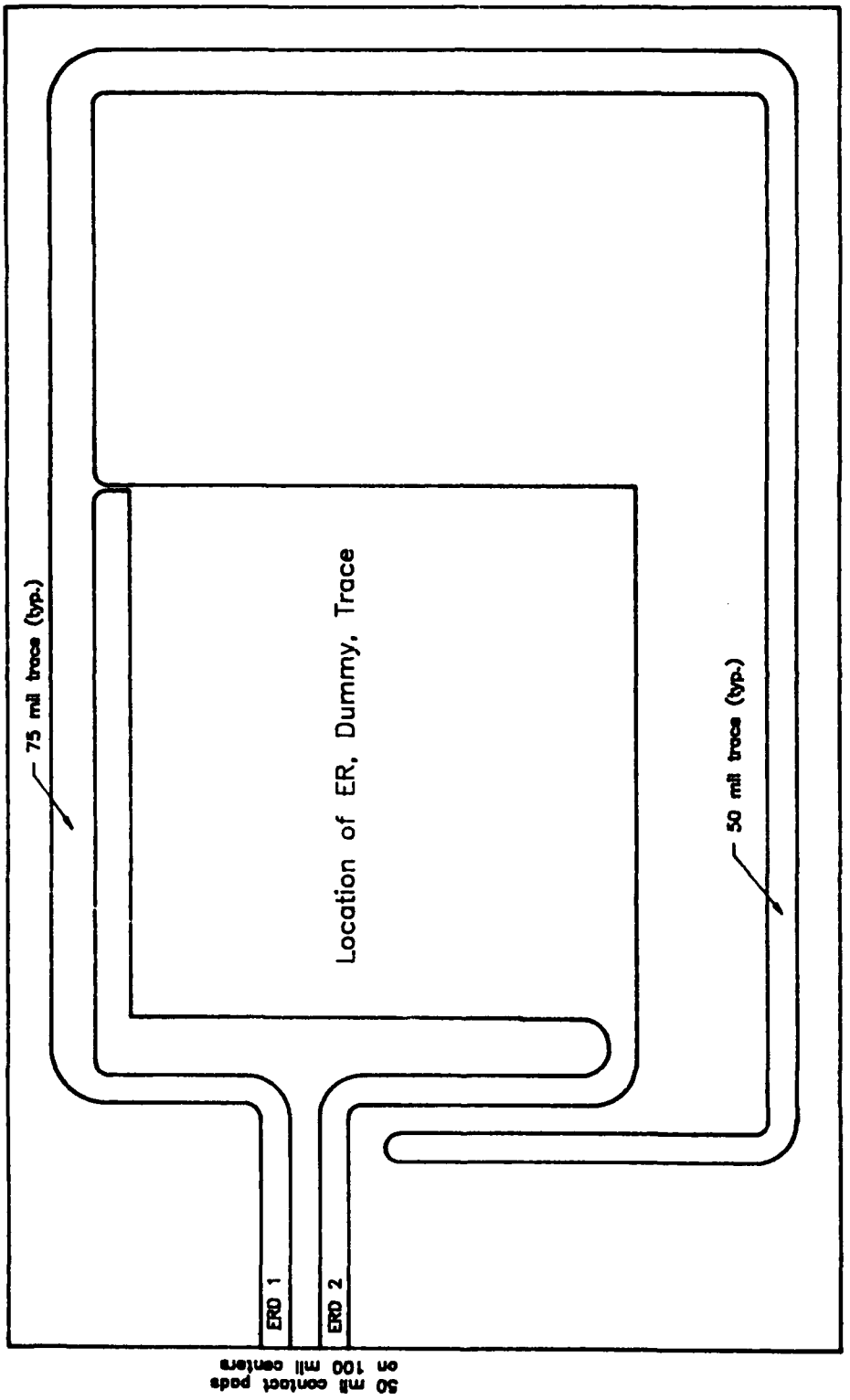

Figure 15. *Back pattern showing bus routing and location of dummy trace.*

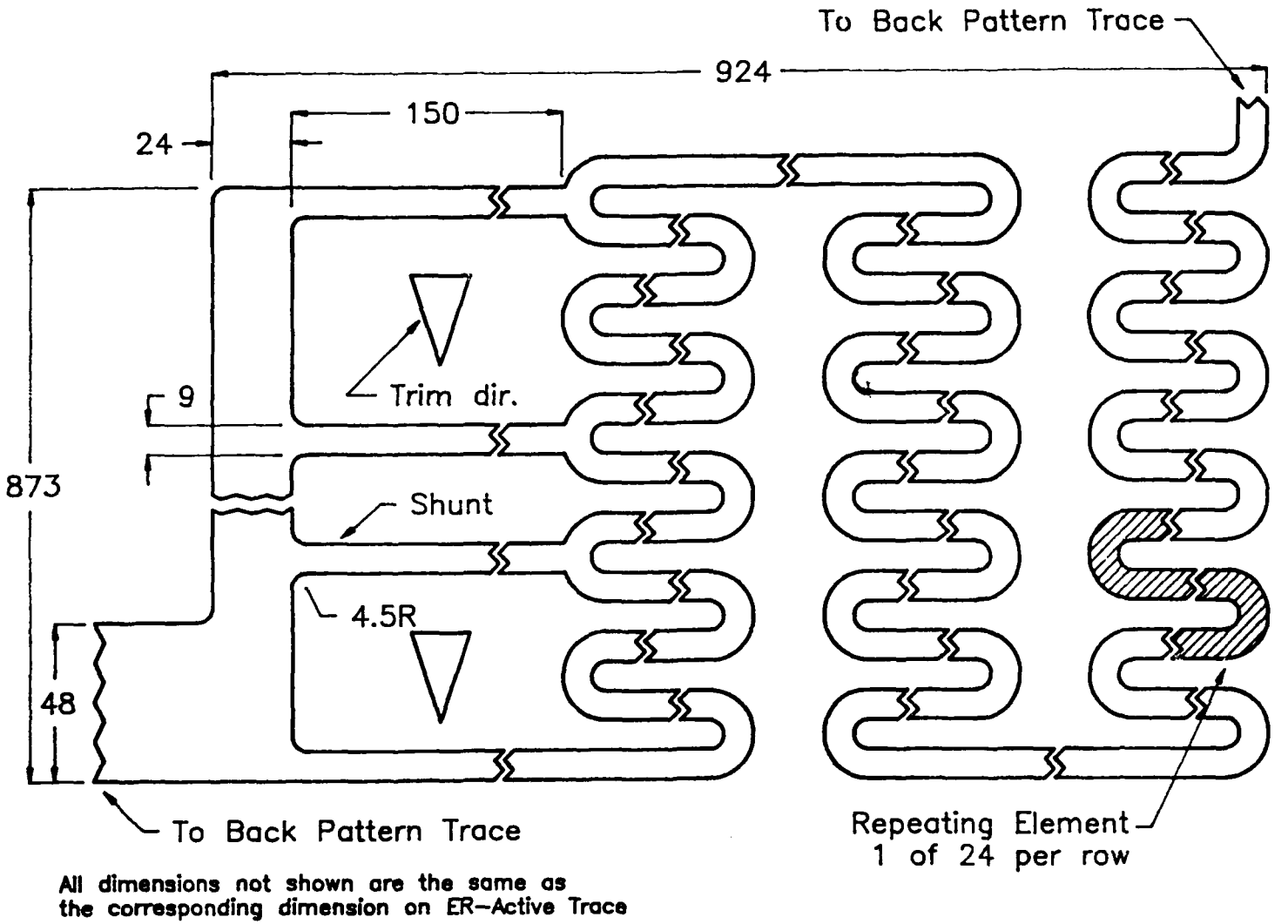

Figure 16. *Detail of Electrical Resistance, Dummy (ERD) compensating trace. Dimensions shown are in mils (0.001 inch).*

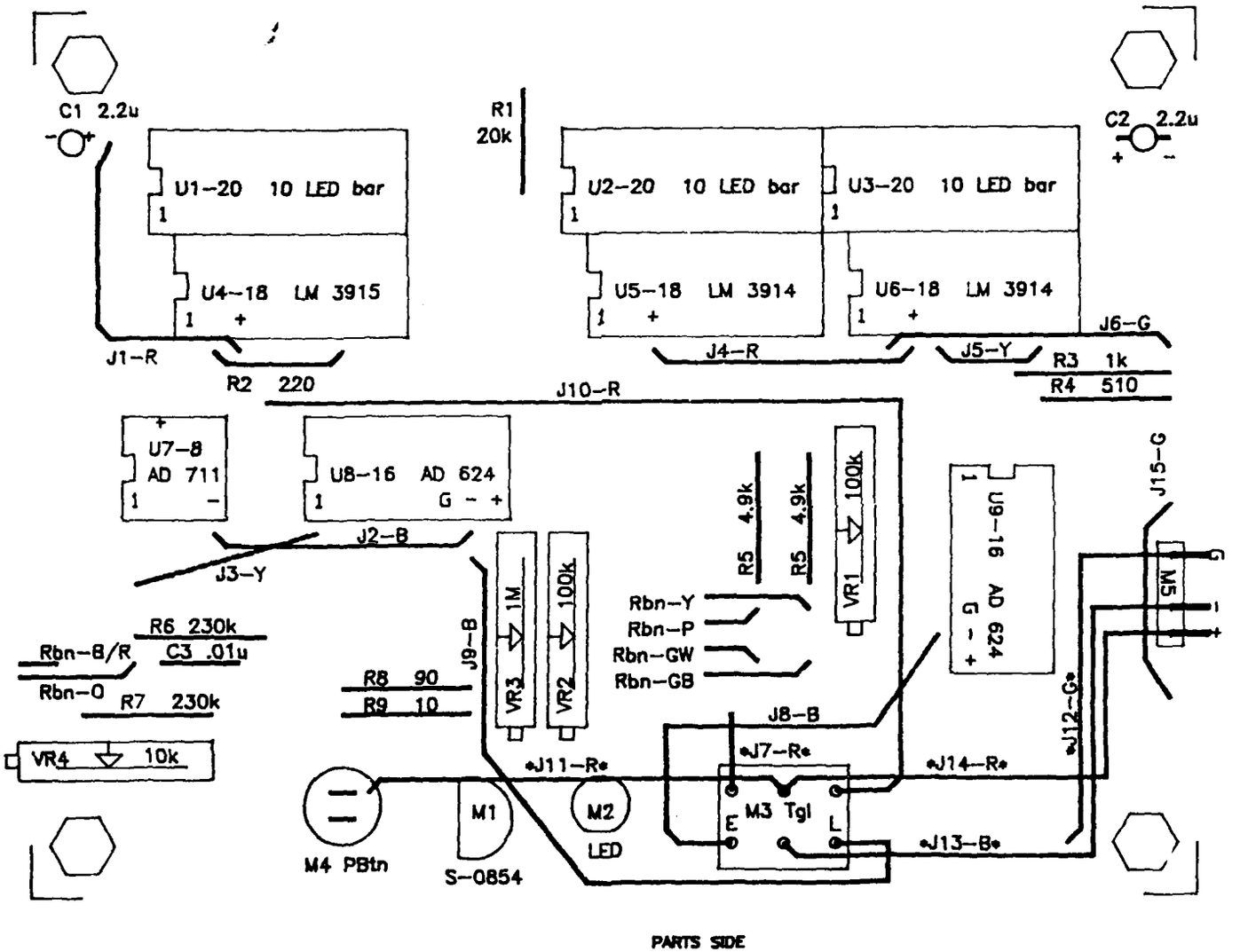

Figure 17. *View of parts side of meter circuit board showing layout of components and jumpers. Jumpers designated by * are routed on the trace side.*

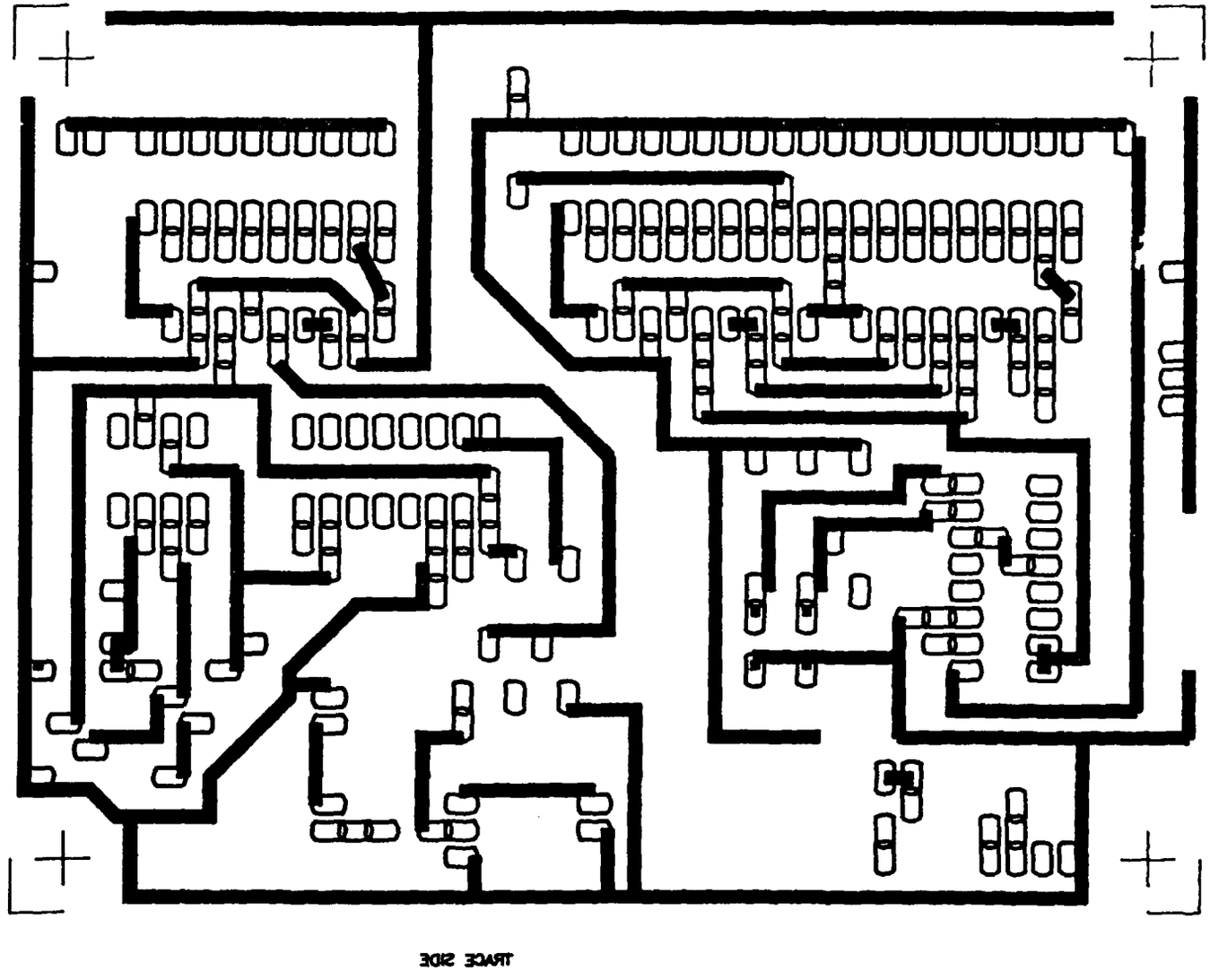

Figure 18. *Circuit board trace as viewed through the parts side. The actual trace is a mirror image of that shown.*

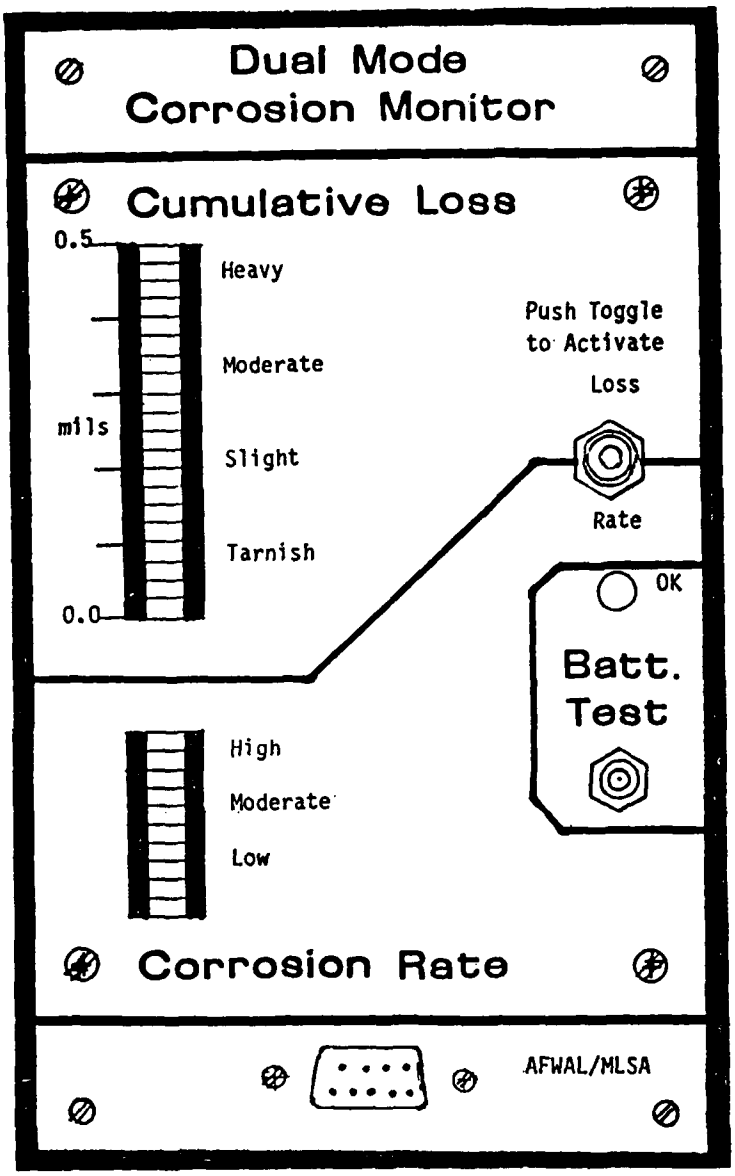

Figure 19. Case label for meter.

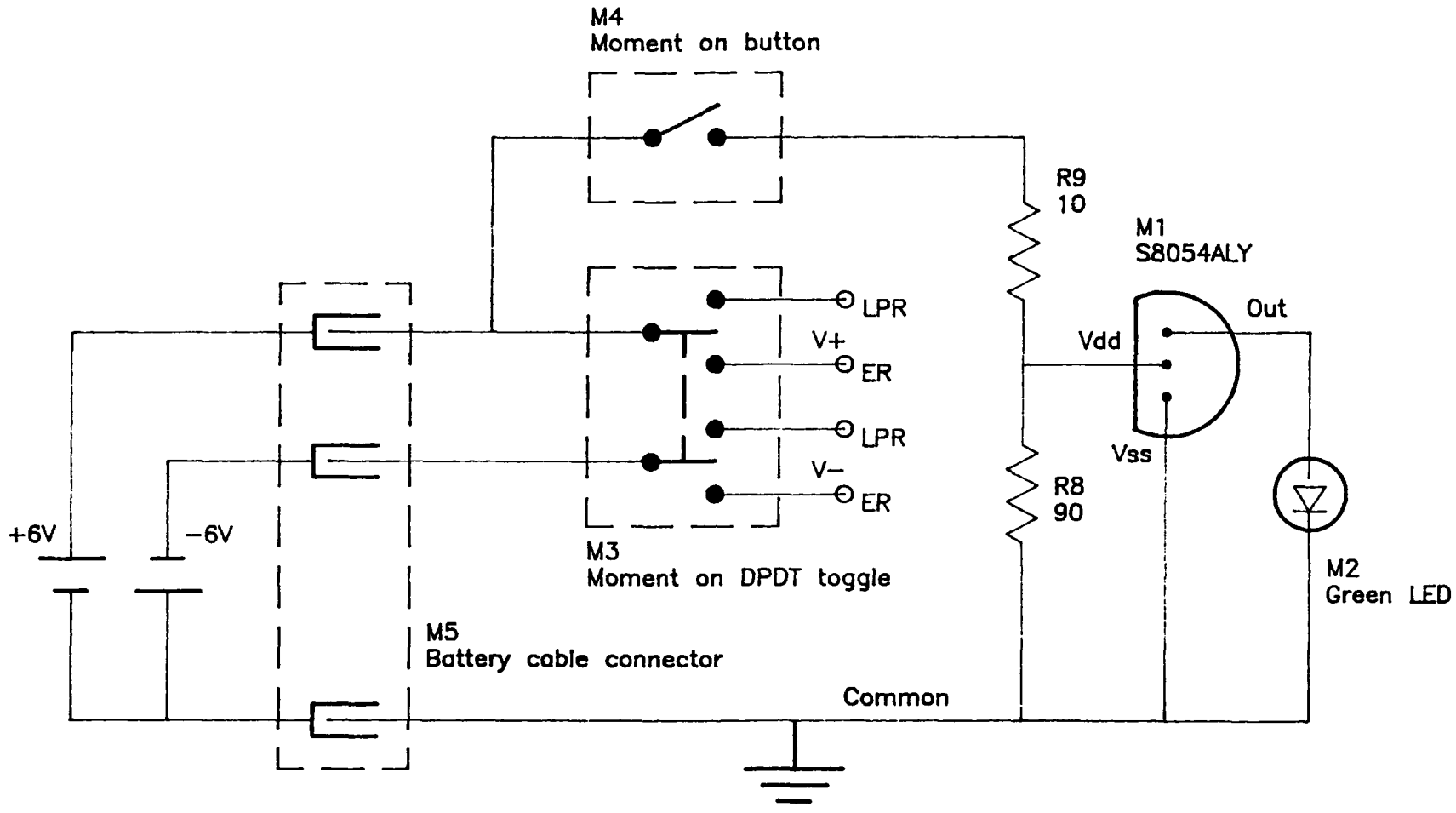

Figure 20. *Schematic of power supply and battery check circuit.*

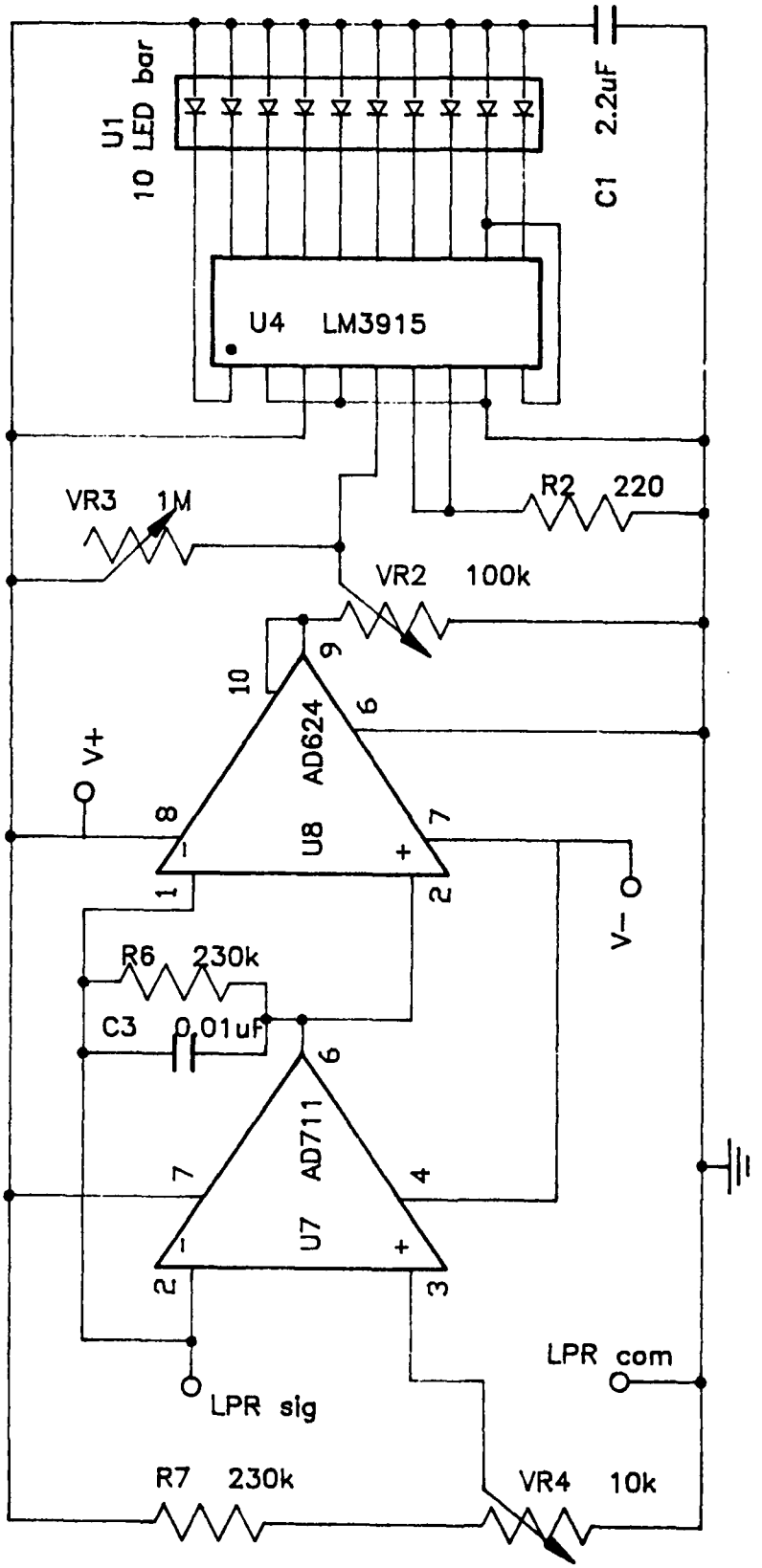

Figure 21. *Schematic of measurement and display circuit for Linear Polarization Resistance sensor (instantaneous corrosion rate).*

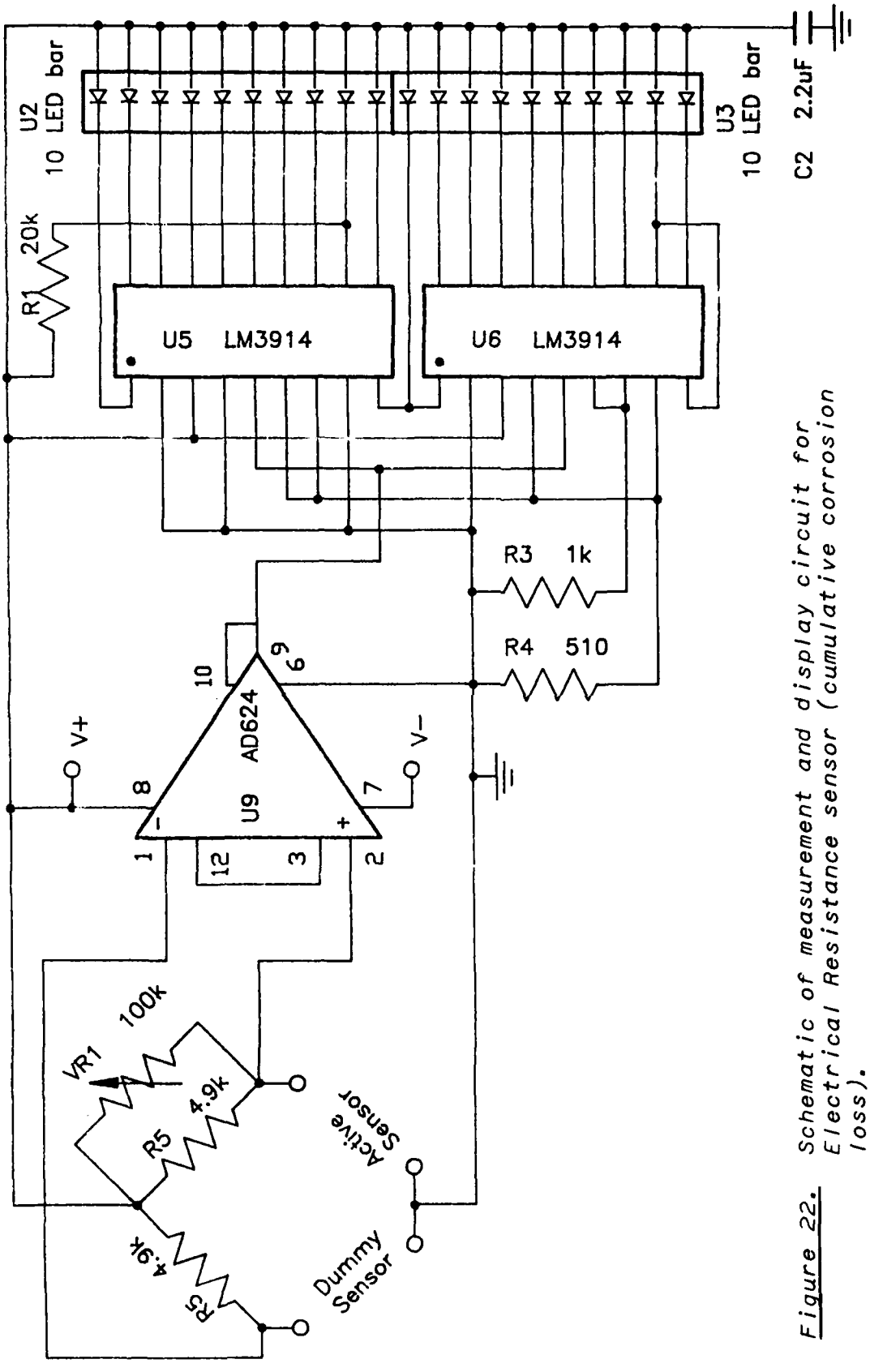

Figure 22. *Schematic of measurement and display circuit for Electrical Resistance sensor (cumulative corrosion loss).*

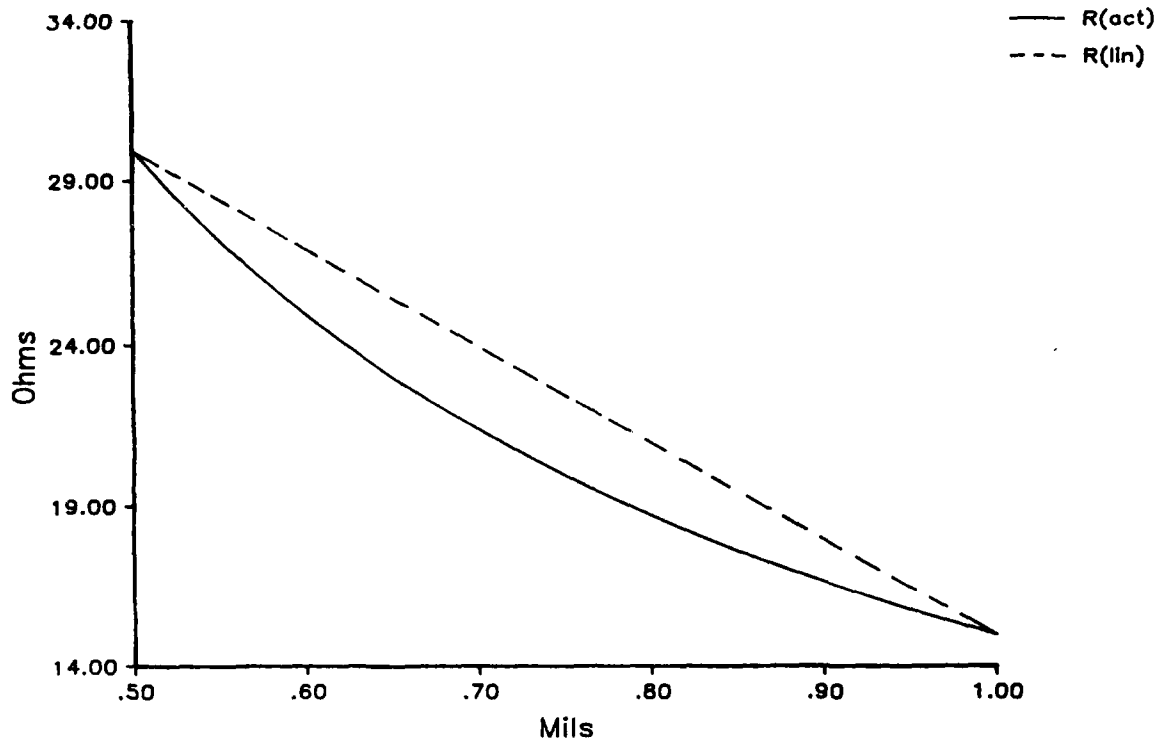

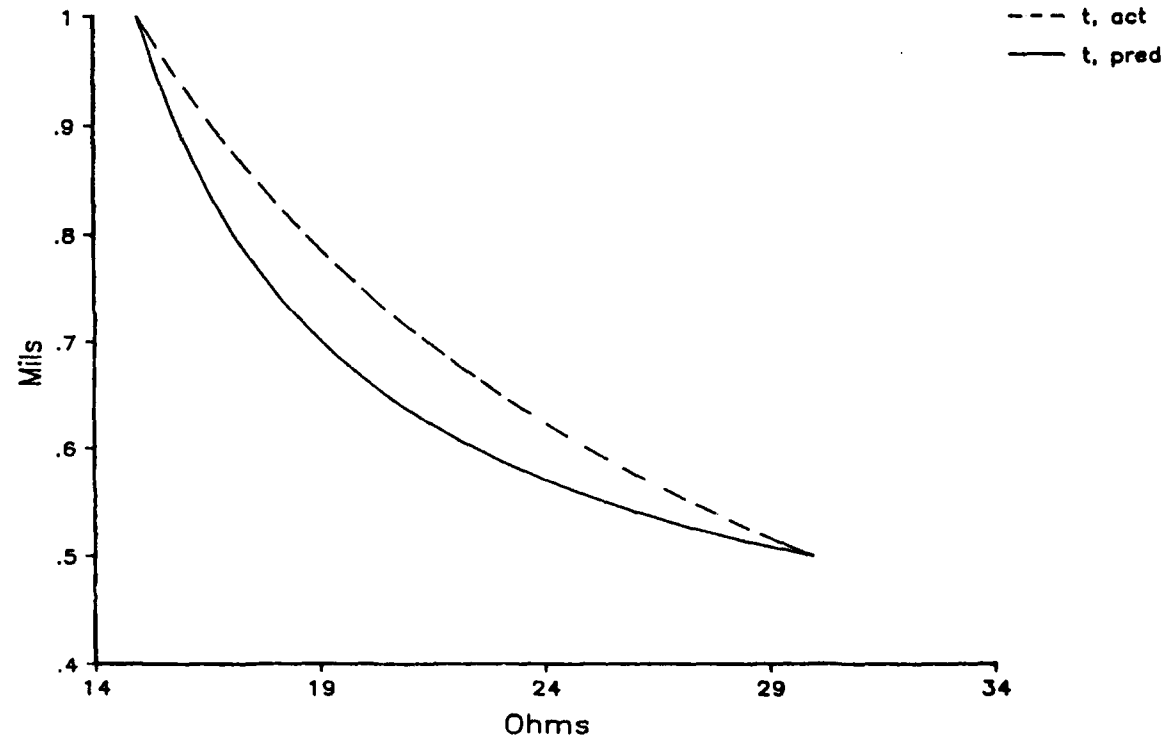

Figure 23. *a. (top): Calculated resistance of ER sensor as a function of foil thickness. Solid line is the actual variation; dashed line is the relationship after linearizing it over a span equal to half the thickness.*

b. (bottom): Predicted foil thickness as a function of foil resistance based on linear relationship (solid); actual thickness as a function of resistance (dashed).

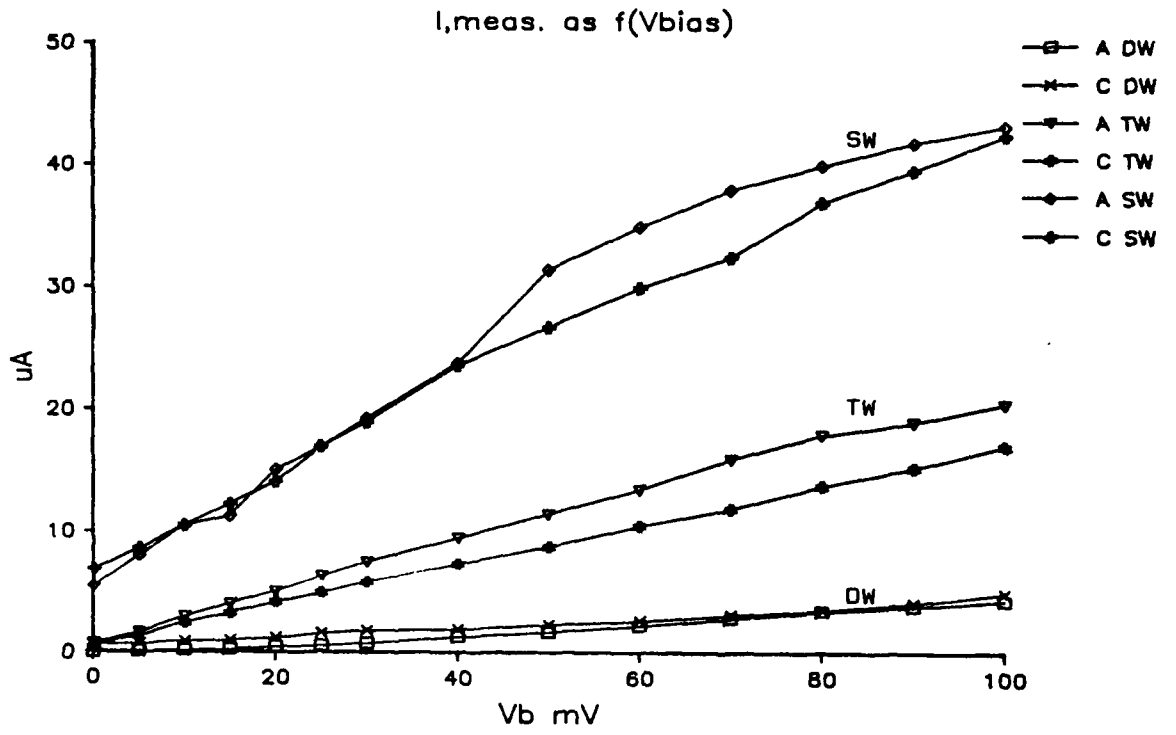

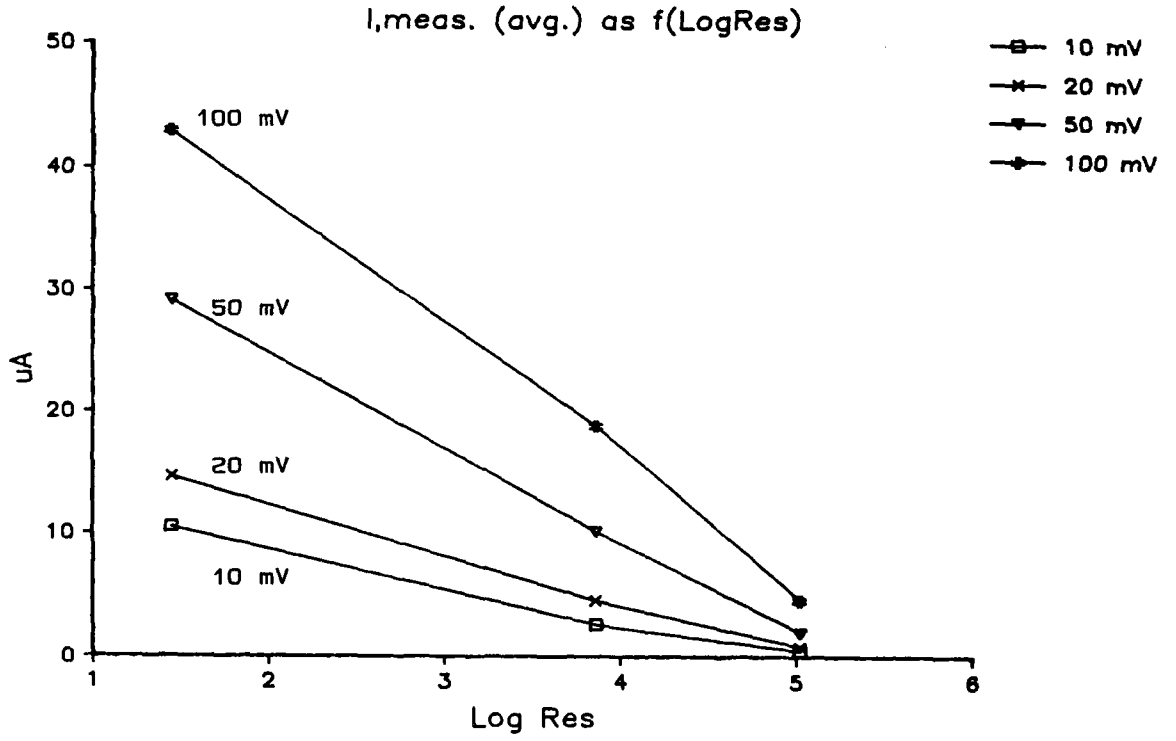

Figure 24. *a. (top): Sensor response current as a function of applied bias voltage in distilled water (DW), tap water (TW) and salt water (SW).*

b. (bottom): Data replotted to show that the response current varies inversely as the log of solution resistivity.

a. *Distilled water*

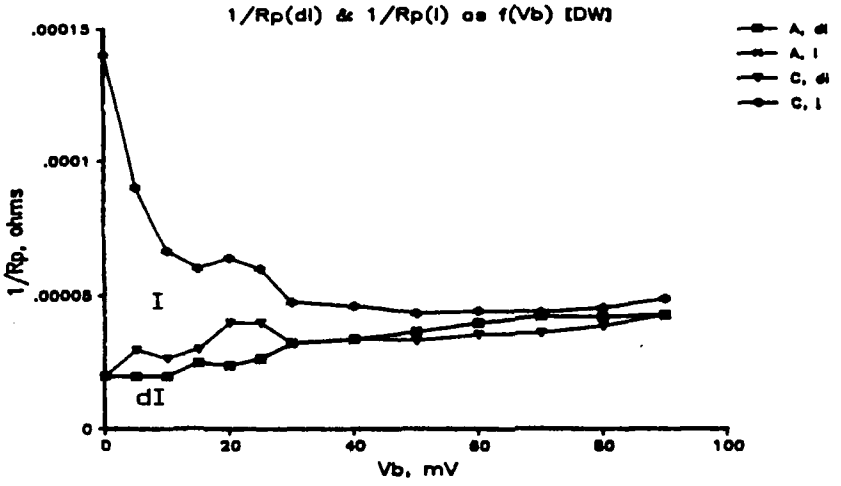

b. *Tap water*

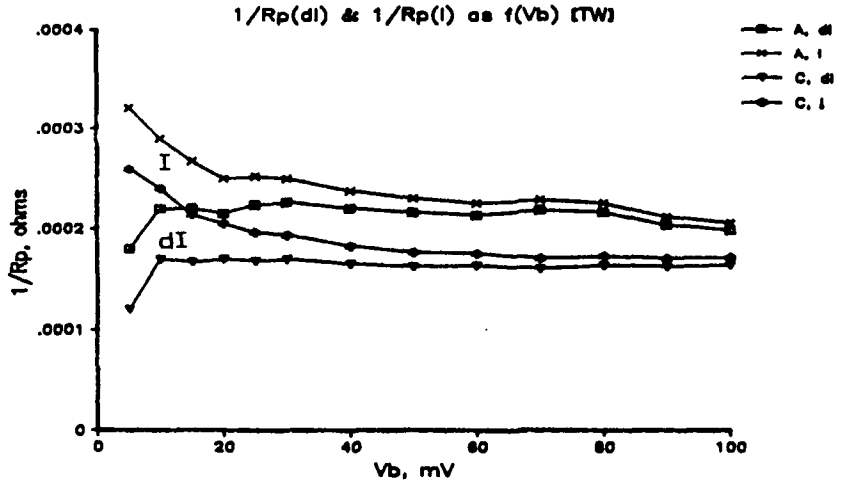

c. *Salt water*

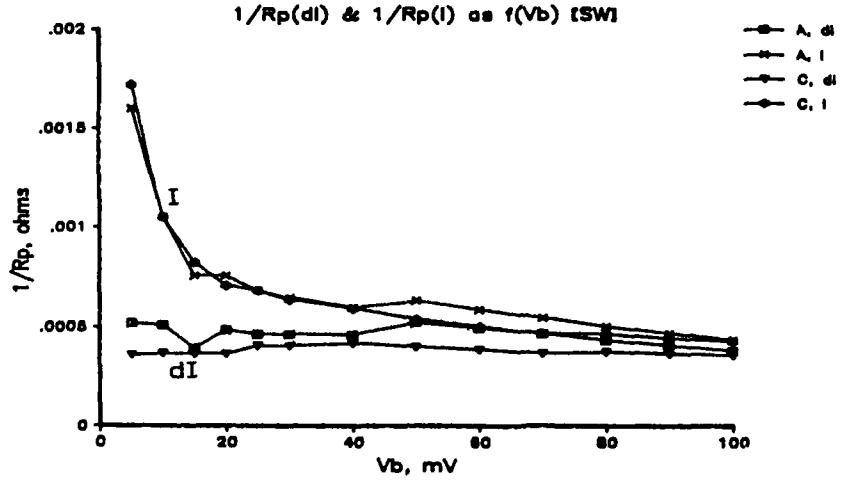

Figure 25. *Inverse polarization resistance as calculated by the single-point (I) and two-point (dI) methods. At bias voltages over 20 mV, the differences are insignificant.*

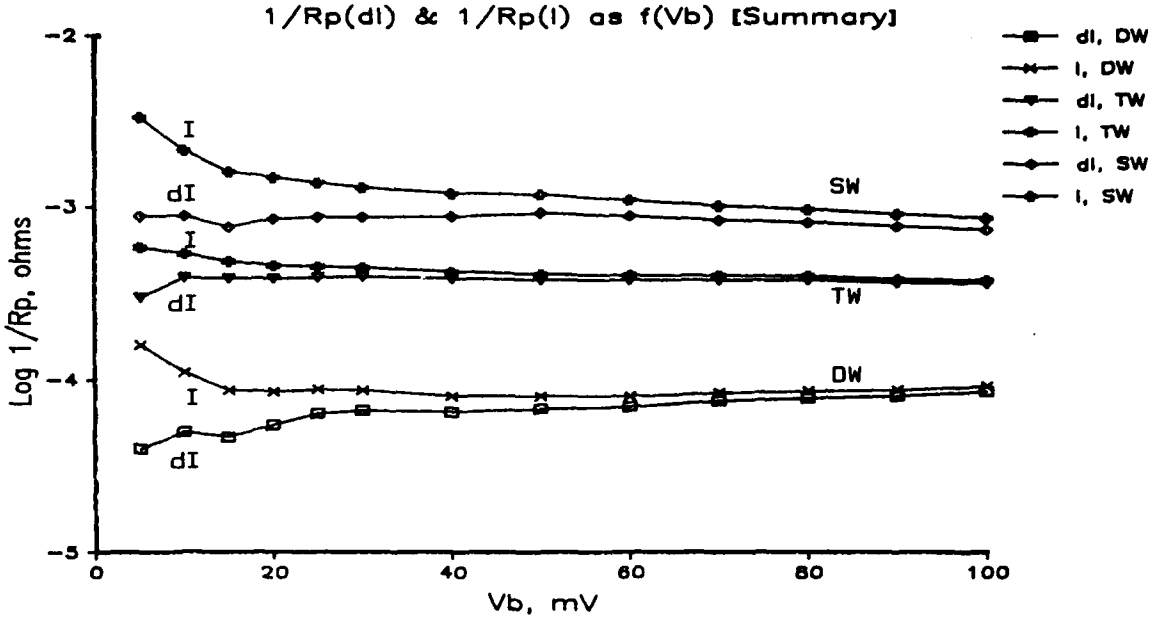

Figure 26. *Data from Figure 25 replotted against the log inverse polarization resistance to facilitate comparison between the three test media.*

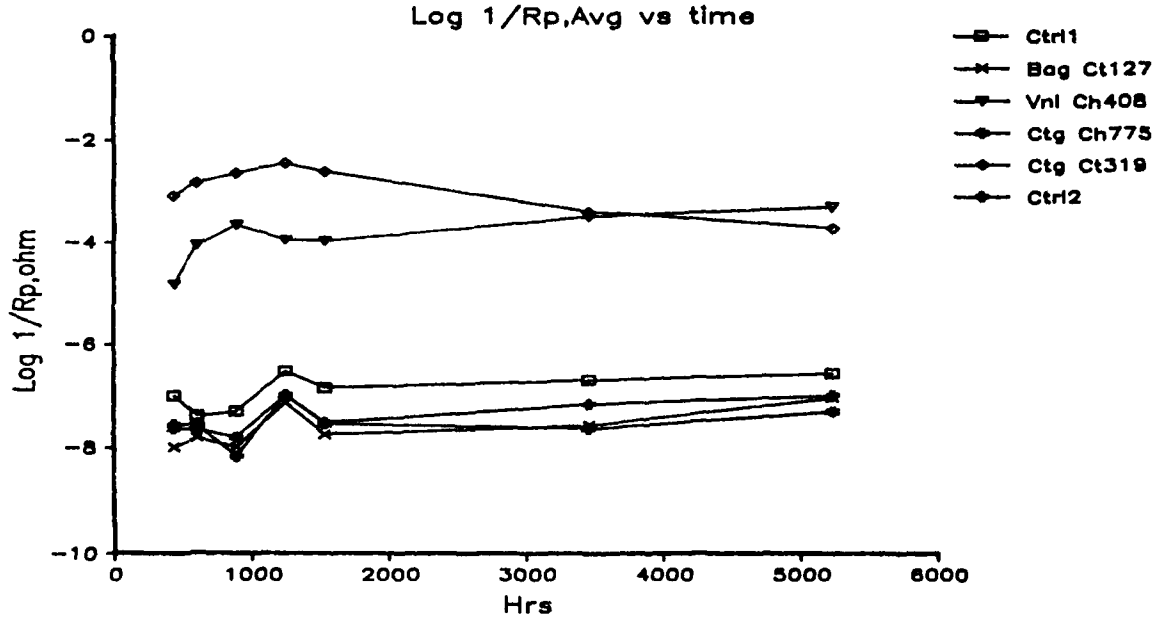

Figure 27. *Data from the packaging study evaluated using the two-point (dI) method. Compare with Figure 10 which is the same data evaluated by the single-point method.*

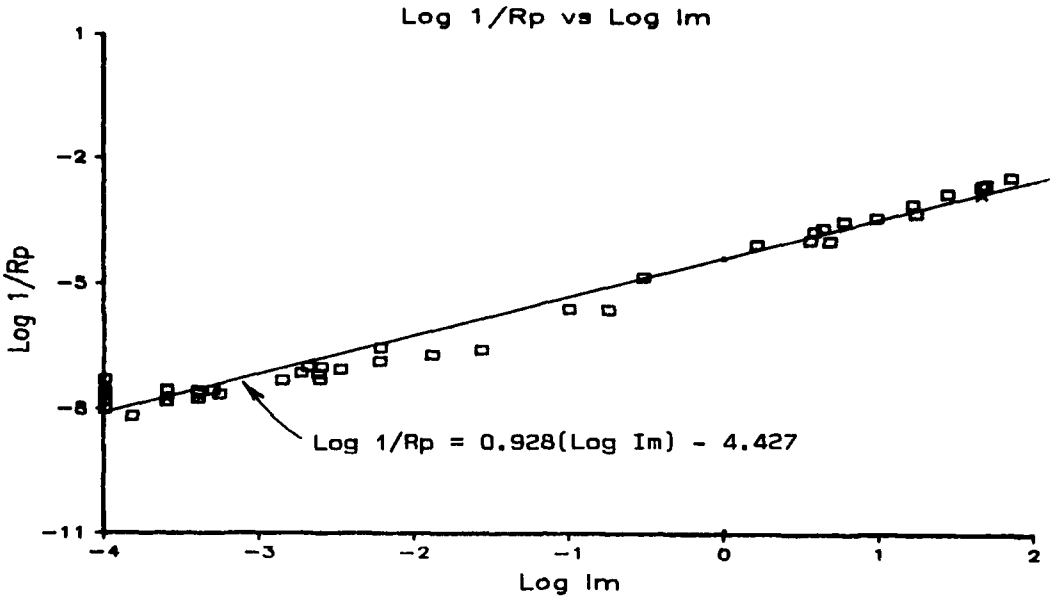

Figure 28. *Correlation of data evaluated by the two-point method (Log 1/Rp) and the single-point method (Log Im). Correlation coefficient in 0.975.*

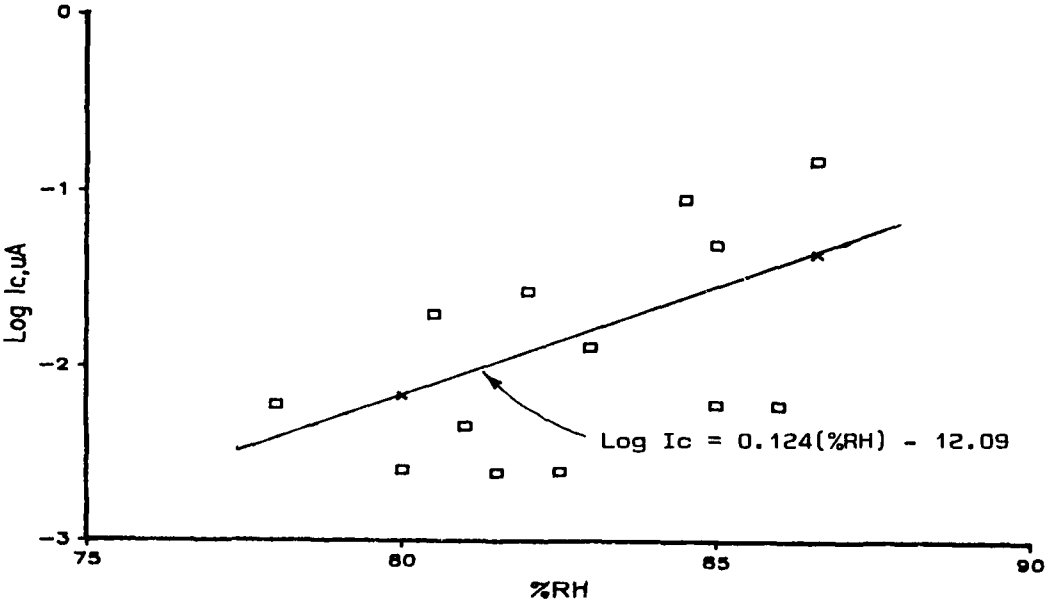

Figure 29. *Data from the packaging study showing correlation between control sensor response and relative humidity in the chamber.*

* U.S.Government Printing Office: 1989 — 648-056/04254